NASA Technical Memorandum 100748

Analytical Derivation and Verification of Zero-Gyro Control for the IUE Satellite

Tiffany Bowles and
John Croft

NOVEMBER 1989

NASA

NASA Technical Memorandum 100748

Analytical Derivation and Verification of Zero-Gyro Control for the IUE Satellite

Tiffany Bowles and
John Croft
Goddard Space Flight Center
Greenbelt, Maryland

NASA
National Aeronautics and
Space Administration

Goddard Space Flight Center
Greenbelt, MD

1989

Analytical Derivation and Verification of

Zero-Gyro Control for the IUE Satellite

PREFACE

The International Ultraviolet Explorer (IUE) satellite was launched January 26, 1978 into a geosynchronous orbit over South America. From its stationary position, the telescope maintains continuous communication with the control centers at the National Aeronautics and Space Administration's (NASA's) Goddard Space Flight Center (GSFC) in Greenbelt, Maryland, and at the European Space Agency's (ESA's) Villafranca del Castillo Satellite Tracking Station in Spain. Since its launch in 1978, the satellite has gradually lost four of the original six gyroscopes in the Inertial Reference Assembly (IRA). In August 1985 the fourth of the original six gyros failed and a two-gyro system developed by NASA-GSFC is ready for use in case of another gyro failure. In the event that the sixth gyro should also fail, a zero-gyro system is being developed. The goal of this system is to provide inertial target pointing without the use of gyroscopes. The satellite has sun sensors to provide attitude information about two of the three axes. It relies upon the exchange of reaction wheel momenta to determine angular position and rate of the third axis.

Table of Contents

Tables

Appendices

I. Background

The original control concept for the IUE satellite was a control system based upon momentum exchange. The satellite's roll, pitch and yaw axes were controlled on a single-axis basis using gyros as sensors and reaction wheels as torquers. The control system hardware also included sun sensors, a hydrazine propulsion system, and an on-board computer.

The reaction wheels are arranged with one wheel on each of the body axes (see figure 1 for satellite axes) and an extra wheel skewed symmetrically with respect to each of the other three axes. The fourth wheel is not necessary for primary control of the satellite but was added as insurance in case any of the other wheels should fail.

There are six gyroscopes on IUE; three are necessary for complete attitude determination and the other three provide for redundancy. The gyros are positioned so that each has some component of body rate about each spacecraft control axis so combining the components of three gyros gives complete attitude determination.

An inertial reference assembly consisting of fine sun sensors and fine error sensors is used for inertial star acquisition, hold and slew maneuvers.

A hydrazine propulsion system was used to adjust the satellite into its initial orbit. It has subsequently helped maintain orbit control and will continue to do so for the life of the satellite. It provides torquing capability for some acquisition modes, delta-V for orbit adjustment maneuvers, and finally, it is used to counteract reaction wheel momentum buildup from environmental disturbances.

FIGURE 1

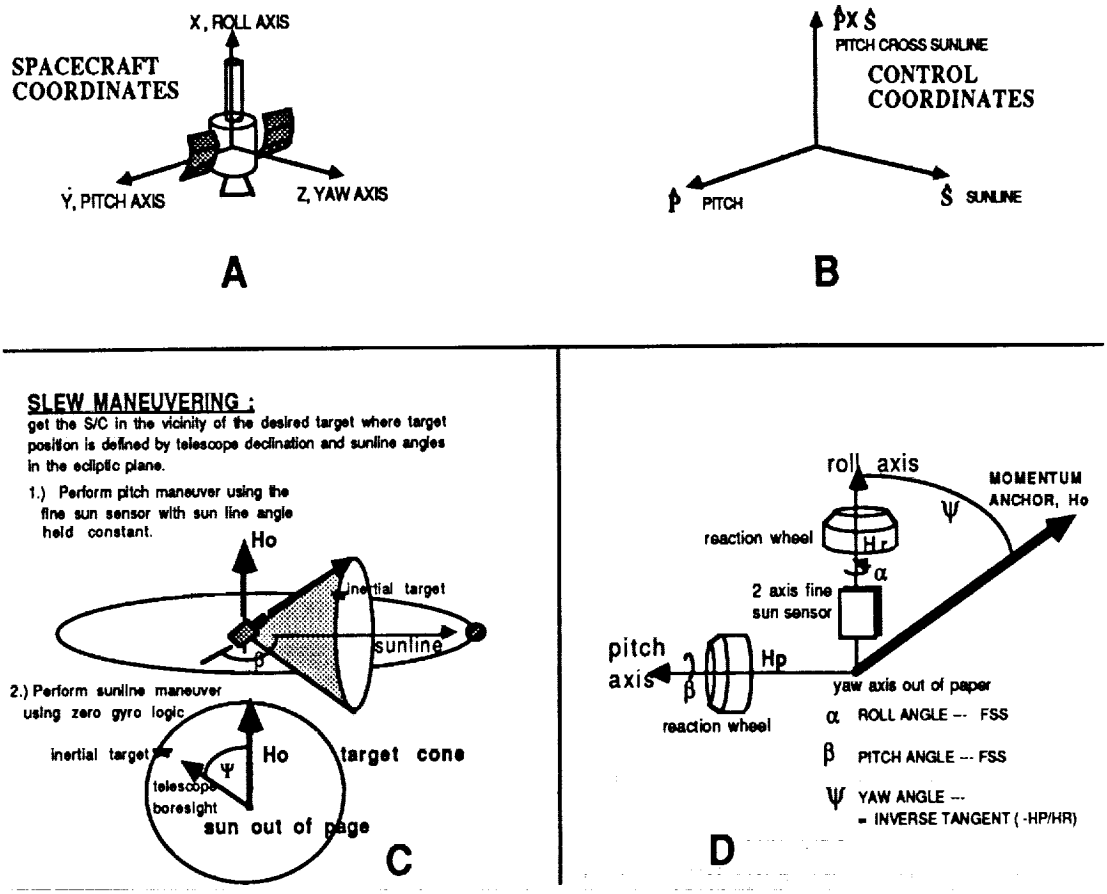

Due to the high altitude of the orbit of IUE, magnetic and gravity gradient unloading techniques could not be used to unload the reaction wheels, and the hydrazine system provided a good alternative. The IUE on-board computer is used for the primary attitude control functions of acquisition, holding and slewing.

Since its launch in 1978, IUE has lost four of its six gyros. A two gyro control system is currently used for control. In the event that the fifth gyro fails, a one gyro system has been developed and is ready for uplink to the satellite. The remainder of this paper addresses a zero gyro control system concept for the IUE satellite.

II. Zero-Gyro Design

The goal of the zero-gyro attitude control system for IUE is to perform sunline and pitch slews to point the telescope boresight to within ±8 arc minutes of an inertial target (see figure 1c) at which

time the fine error sensor control law takes over. (The fine error sensor is currently in operation and has a field of view of 16 arc minutes.) When all gyros aboard the IUE satellite have failed, we will only be able to rely on the fine sun sensors and fine error sensor for satellite attitude information. IUE is equipped with two fine sun sensors to provide angle information about the pitch and p x s axes (the p x s axis is the cross product of the pitch and sunline axes, see figure 1a,b) leaving us with no means to measure angular position along the sunline axis.

The zero gyro system uses the fine sun sensor to provide position information for control of the pitch and pxs axes (figure 1d). Note that at beta=90 degrees, the PxS axis is the roll axis. This sensor information is used to derive standard position and derived rate control laws. In order to explain our method for controlling the sunline axis, let us first start with a simple case by aligning the yaw axis with the sunline. Here a sunline maneuver is confined to the pitch-p x s plane (see figure 2).

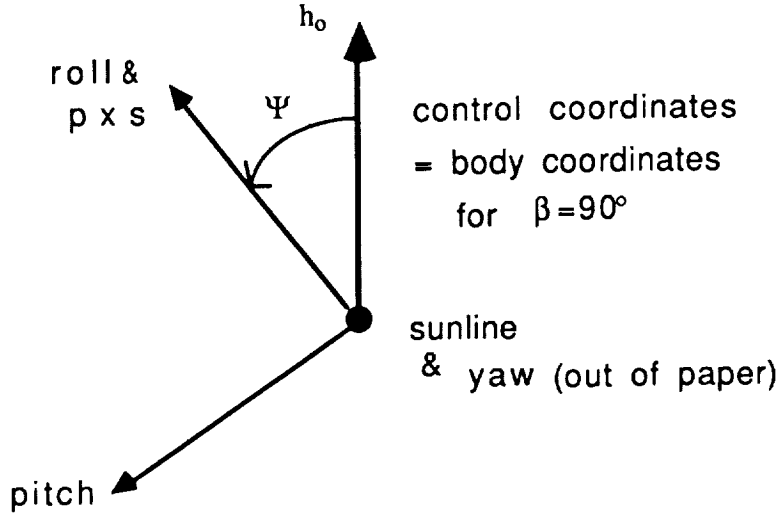

Figure 2

Thrusters will be used to place a momentum 'anchor', h_o, along the north ecliptic pole. It is possible to compute the sunline (yaw axis for $\beta=90°$) angle using the satellite wheel momenta information from the reaction wheels. From the law of conservation of

momentum it is known that as the satellite rotates, h_o will be transferred from one axis to another (assuming that external torques are negligible). If the satellite is considered to be inertially fixed, the satellite momentum is equal to the reaction wheel momentum; therefore, as the satellite rotates the momentum is transferred amongst the three wheels.

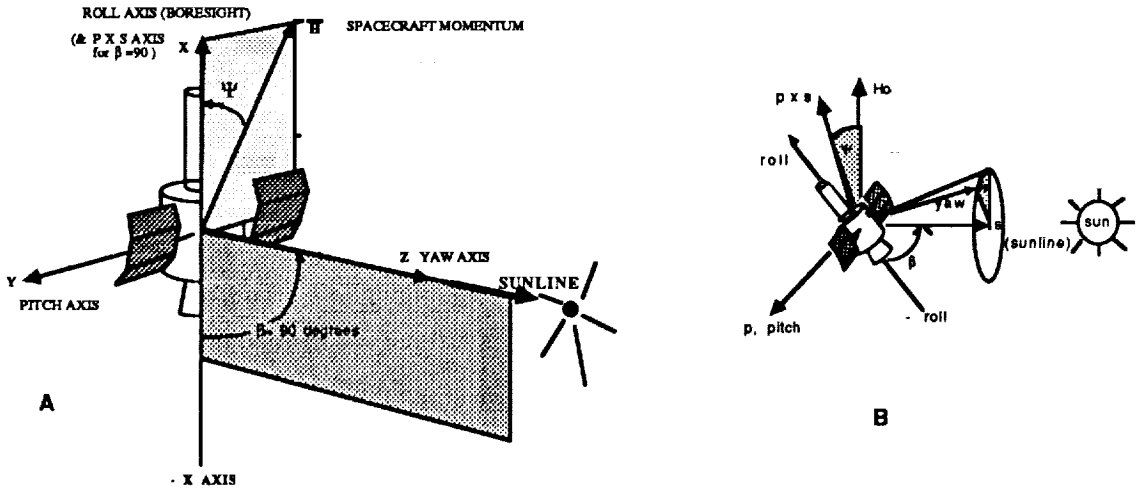

FIGURE 3

Looking at the inertial coordinate system, we can see that the angle psi, rotation about the sunline axis (yaw axis for $\beta=90°$), lies in the x-y plane (see figure 3a). For a pure yaw maneuver, the case where beta is 90 degrees, the transfer of momentum is confined to the pitch and roll axes. Control computations become more difficult when momentum transfer involves all three axes (see figure 3b). The first case to consider is when the spacecraft is positioned with its yaw axis along the sunline, $\beta=90°$. With the yaw axis aligned along the sunline, the control coordinate system coincides with the spacecraft coordinate system making satellite control easier to visualize.

The desired control law is derived from the symbolic block diagram shown in Appendix A. It uses both the angular position of the satellite and the angular rate to determine the desired torque. For sunline (yaw at beta=90 degrees) control, the torque about the sunline axis, T sunline is:

$$T_{sunline} = A(\psi - \psi_c) + C\dot{\psi} \qquad (1)$$

where Ψ = Sunline angle

Ψ_c = Commanded Sunline angle

$\dot{\Psi}$ = Sunline rate

A = position gain = $I_z \omega^2_{n\ sunline}$

C = rate gain = $2 I_z \zeta \omega_{n\ sunline}$

The position and rate gain come from the standard proportional-plus-derivative (PD) controller definitions for the approximation of a second-order system. I_z is the moment of inertia about the yaw axis, ω_n is the sunline control bandwidth, and ζ is the sunline damping ratio (see appendix C for values).

Figure 4 shows how the angle psi is defined. From trigonometry we have the relation tan Ψ = -Hp/Hr, and from that it is easy to see

$$\Psi = \tan^{-1}(-Hp/Hr). \qquad (2)$$

Hp = pitch wheel momentum

Hr = roll wheel momentum

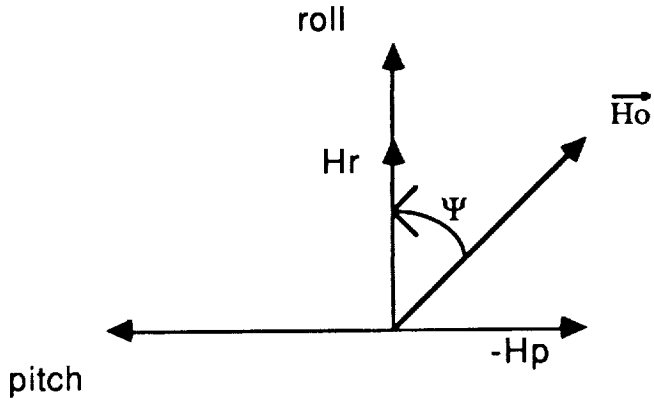

Figure 4

The derivative of psi, the sunline rate, comes from the two relations

$Hr = Ho \cos \Psi$ and (3a)

$Hp = -Ho \sin \Psi$. (3b)

Taking the derivative of equation 3b gives $\dot{Hp} = -Ho \cos \Psi \dot{\Psi}$, and the

substitution of Hr from equation 3a results in

$$\dot{\Psi} = -\frac{\dot{H}_p}{H_r}. \qquad (4)$$

With the substitutions of equations 2 and 4 and the introduction of commanded sunline angle (T sunline=T yaw=Tz), the control law in equation 1 becomes

$$Tz = -A\left(\arctan\frac{Hp}{Hr} - \Psi c\right) - C\frac{\dot{H}p}{Hr}. \qquad (5)$$

The small angle approximations explained in Appendix B, can further simplify the general control law to

$$Tz = -A\left(\frac{Hp}{Hr} + \tan\Psi_c\right)(\cos\Psi_c)^2 - C\frac{\dot{H}p}{Hr} \qquad (6)$$

The control law for the pitch axis at β=90 degrees is based on position and derived rate from the fine sun sensor (Tp = T pitch).

$$T_p = Kp(\beta - \beta_{cmd}) + Kr\frac{(\beta_{present} - \beta_{past})}{\Delta t} \qquad (7)$$

where Kp = position gain
Kr = rate gain

A p x s angle of zero degrees is maintained by a position and derived rate control from the fine sun sensor.

The only modifications needed for the general sunline control law for β=90° are due to the presence of singularities in the tangent function. In trying to command various sunline maneuvers from Ψ = 0° to 360° it will be necessary to pass through those singularities. To combat this problem, sunline control has been broken into four quadrants (see figure 5) with a modified control law for each quadrant. The four quadrant sunline control laws are as follows:

Note : at beta=90 degrees , Tq sunline = Tz

$$\text{Quad I: Tq sunline} = -A\left(\frac{Hp}{|Hr|} + \tan\Psi_{com}\right)(\cos\Psi_{com})^2 - C\frac{\dot{H}p}{|Hr|} \qquad -45° \le \Psi_{com} \le 45° \qquad (8a)$$

$$\text{Quad II: Tq sunline} = -A\left(\frac{Hr}{|Hp|} - \cot\Psi_{com}\right)(\sin\Psi_{com})^2 - C\frac{\dot{Hr}}{|Hp|} \qquad 45°\leq\Psi_{com}\leq135° \quad (8b)$$

$$\text{Quad III: Tq sunline} = A\left(\frac{Hp}{|Hr|} - \tan\Psi_{com}\right)(\cos\Psi_{com})^2 + C\frac{\dot{Hp}}{|Hr|} \qquad 135°\leq\Psi_{com}\leq225° \quad (8c)$$

$$\text{Quad IV: Tq sunline} = A\left(\frac{Hr}{|Hp|} + \cot\Psi_{com}\right)(\sin\Psi_{com})^2 + C\frac{\dot{Hr}}{|Hp|} \qquad 225°\leq\Psi_{com}\leq315° \quad (8d)$$

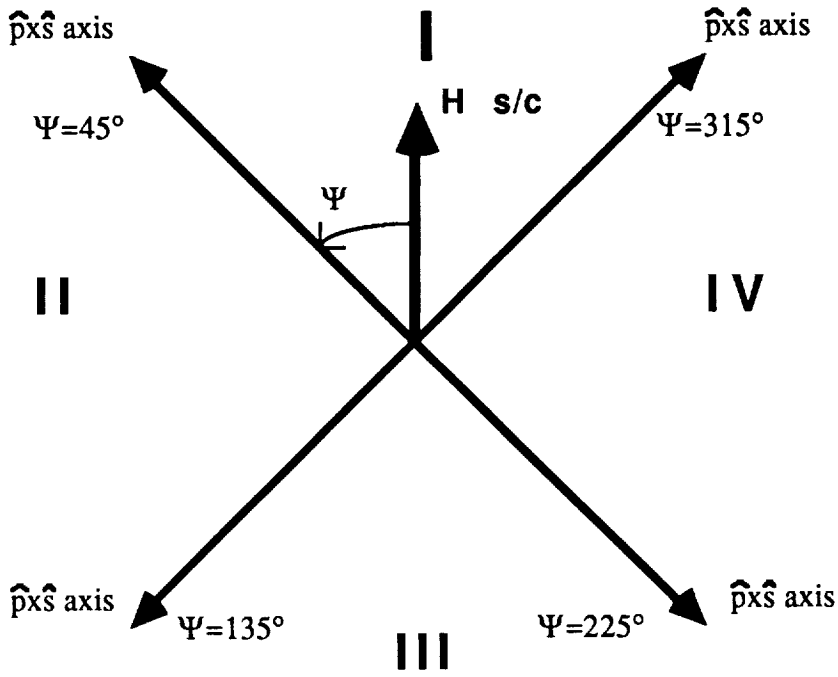

Figure 5

ORIENTATION OF PxS AXIS WITH RESPECT TO MOMENTUM ANCHOR AS A FUNCTION OF SUNLINE ANGLE

The roll and yaw control laws become more complicated when the spacecraft yaw axis is no longer aligned with the sunline ($\beta\neq90°$) because it is necessary to work in two different coordinate frames, the body coordinates and the control coordinates (see figure 3b). The control torques are logically computed in the control coordinate frame where the bandwidth and damping ratio are defined (see Appendix C). However, the control law is dependent upon body inertias, which are intrinsic to the body coordinate frame, so the

reaction wheel momenta must first be expressed in control coordinates. After the control torques have been determined in the control coordinate frame it is necessary to convert them to body frame torques (i.e. commands to the reaction wheels). This requires several modifications to the original control law.

It is first necessary to express the reaction wheel momenta in control coordinates. This can be done through a simple coordinate transformation shown below. With these momenta it is now possible to compute the control torques in control coordinates (T_{pxs}, T_{pitch}, $T_{sunline}$ defined on page 12, equations 18, 19, 20).

$$\begin{bmatrix} Hpxs \\ Hp \\ Hs \end{bmatrix} = \begin{bmatrix} \sin\beta & 0 & \cos\beta \\ 0 & 1 & 0 \\ -\cos\beta & 0 & \sin\beta \end{bmatrix} \begin{bmatrix} Hroll \\ Hpitch \\ Hyaw \end{bmatrix}$$

control body

In order to implement the necessary control torques they must be transformed into body coordinates. It is desirable to use a coordinate transformation to convert control frame accelerations into body frame accelerations instead of transforming the control torques (see appendix C for conversion of torque to acceleration). These accelerations are now transformed into the body frame through the following transformation.

$$\begin{bmatrix} Aroll \\ Apitch \\ Ayaw \end{bmatrix} = \begin{bmatrix} \sin\beta & 0 & -\cos\beta \\ 0 & 1 & 0 \\ \cos\beta & 0 & \sin\beta \end{bmatrix} \begin{bmatrix} Apxs \\ Apitch \\ Asun \end{bmatrix}$$

body control

Recomputing the body torques from the transformed accelerations with the familiar relation $T = I\alpha$ gives the following torques for quadrant I control:

$Troll = \sin\beta[rkp\ \alpha + rkr\ \dot{\alpha}]$

$$-\cos\beta\left[-A\left(\frac{Hp}{|Hr\sin\beta+Hy\cos\beta|}+\tan\Psi_c\right)(\cos\Psi_c)^2-C\left(\frac{\dot{H}p}{|Hr\sin\beta+Hy\cos\beta|}\right)\right]\frac{Iroll}{Iyaw} \quad (9)$$

$$Tpitch=kp(\beta-\beta_c)+kr\,\dot{\beta} \quad (10)$$

$$Tyaw=\cos\beta[kp\,\alpha+kr\,\dot{\alpha}]\frac{Iyaw}{Iroll}$$

$$+\sin\beta\left[-A\left(\frac{Hp}{|Hr\sin\beta+Hy\cos\beta|}+\tan\Psi_c\right)(\cos\Psi_c)^2-C\left(\frac{\dot{H}p}{|Hr\sin\beta+Hy\cos\beta|}\right)\right]. \quad (11)$$

The control laws for the remaining three quadrants can be developed with the same series of transformations.

III. Stability Analysis

After developing the control laws it is necessary to perform a stability analysis to determine the range of control law gains that provide stable control of the satellite. If the nominal gains chosen are adequately stable, the next step is to determine acceptable gain margins for slewing and settling. The stability analyses were done in two stages. The control laws for operation at $\beta=90°$, $\Psi= 0°$ to 360° were analyzed first (see block diagram in figure 6), and once working gain margins were established by linear analysis and linear and non-linear simulations, analysis began on the $\beta\neq90°$, $\Psi = 0°$ to 360°, control laws thereby covering stability of the entire operational range.

A. Linear Analysis

The equations of motion for each body frame axis are derived using Euler's equation and setting the external torques to zero.

$$\dot{\overline{H_o}} = -\overline{\omega} \times H_o \quad (12)$$

It is known that the momentum on each axis is a sum of the spacecraft momentum and the reaction wheel momentum. The torque is the derivative of the momentum and can be represented as

$$\dot{H}_x = I_x\dot{\omega}_x + \dot{h}_x \quad (13a)$$

$$\dot{H}_y = I_y\dot{\omega}_y + \dot{h}_y \quad (13b)$$

$$\dot{H}_z = I_z\dot{\omega}_z + \dot{h}_z \quad (13c)$$

where H = spacecraft momentum, and h = wheel momentum.

BLOCK DIAGRAM FOR BETA=90 DEGREES

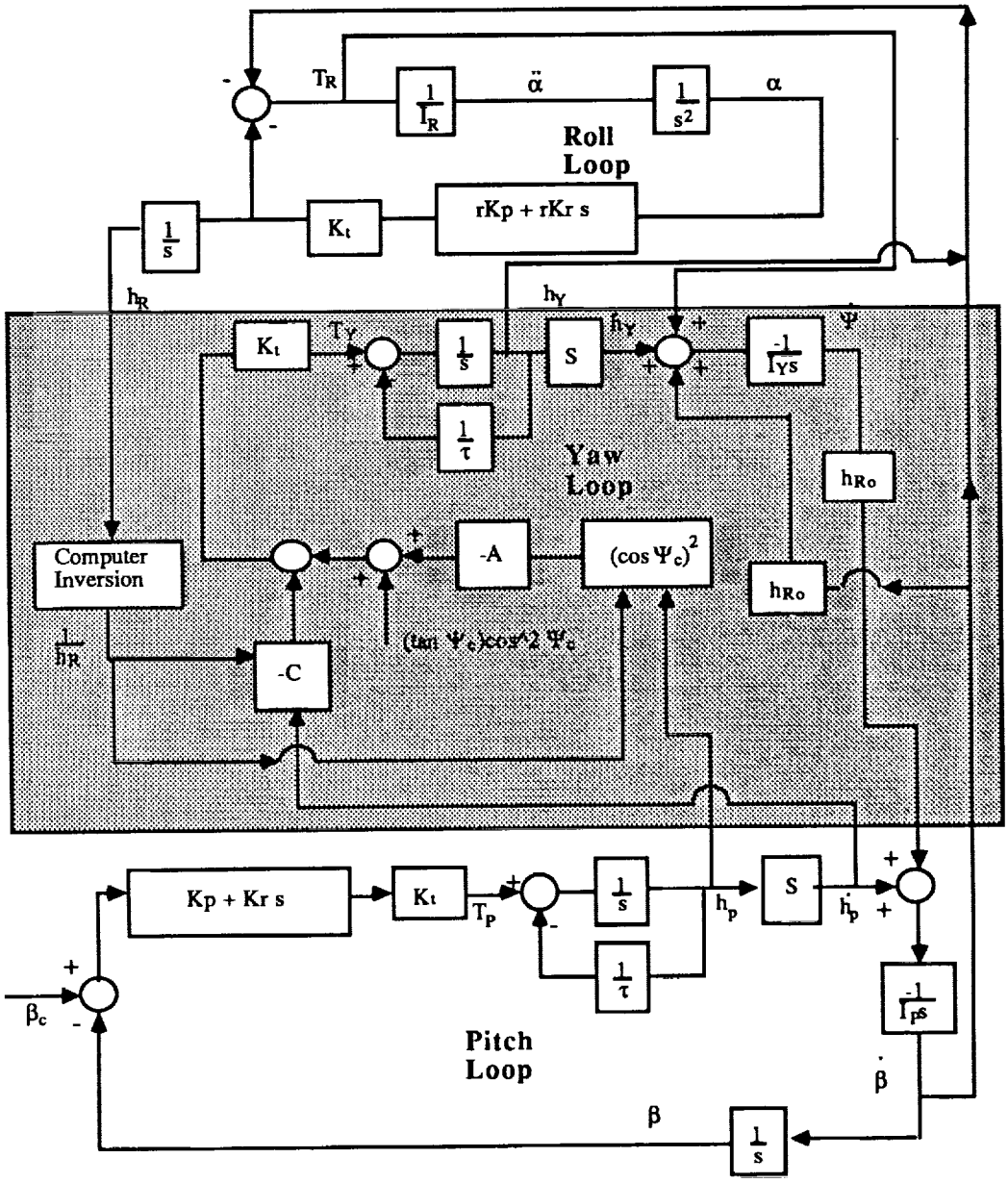

Figure 6

Expanding the ωxH term on the right side of equation 12 above leads to

$$\overline{\omega} \times \overline{H_o} = (\omega_y H_z - \omega_z H_y)\hat{i} + (\omega_z H_x - \omega_x H_z)\hat{j} + (\omega_x H_y - \omega_y H_x)\hat{k}$$

which can be combined with the momentum equations 13a-c into three equations for roll, pitch, and yaw.

$$0 = I_x \dot{\omega}_x + \dot{h}_x + \omega_y H_z - \omega_z H_y \qquad \text{roll}$$

$$0 = I_y\dot{\omega}_y + \dot{h}_y + \omega_z H_x - \omega_x H_z \qquad \text{pitch}$$

$$0 = I_z\dot{\omega}_z + \dot{h}_z + \omega_x H_y - \omega_y H_x \qquad \text{yaw}$$

Under the assumption that the spacecraft is inertially fixed, the first derivatives of the direction angles (alpha, beta, and psi) can be substituted for the spacecraft rates ω_x, ω_y, and ω_z in the equations above. It is also necessary to allow for some initial momentum bias on each of the reaction wheels. Let $h=h_O+\Delta h$ on each axis where h_O is the steady-state momentum and Δh is the momentum input from the reaction wheels. These modifications bring us to the three equations of motion.

$$0 = I_x\ddot{\alpha}+\Delta\dot{h}_x+\dot{\beta}(I_z\dot{\psi}+h_{zo}+\Delta h_z)-\dot{\psi}(I_y\dot{\beta}+h_{yo}+\Delta h_y) \qquad (14)$$

$$0 = I_y\ddot{\beta}+\Delta\dot{h}_y+\dot{\psi}(I_x\dot{\alpha}+h_{xo}+\Delta h_x)-\dot{\alpha}(I_z\dot{\psi}+h_{zo}+\Delta h_z) \qquad (15)$$

$$0 = I_z\ddot{\psi}+\Delta\dot{h}_z+\dot{\alpha}(I_y\dot{\beta}+h_{yo}+\Delta h_y)-\dot{\beta}(I_x\dot{\alpha}+h_{xo}+\Delta h_x) \qquad (16)$$

The control equations for $\beta=90°$ are developed by using the torque equations 6 and 7 along with the torque on the wheels.

$$T = \Delta\dot{h} = I_\omega(\dot{\omega}_{s/c} + \dot{\omega}_{wheel}) \qquad (17)$$

The product $I_\omega\dot{\omega}_{s/c}$ is small enough in comparison with the other term to be considered negligible, and for practical purposes may be discarded. Combining the two torque equations 7 and 17 for both the roll and pitch axes will give the control equations for those axes. The yaw control torque was explained earlier (equations 1-6) and, along with the wheel torque leads to the yaw control equation.

$$\Delta\dot{h}_x = RKp\,\alpha + RKr\,\dot{\alpha} \qquad \text{roll} \qquad (18)$$

$$\Delta\dot{h}_y = Kp(\beta - \beta_c) + Kr\,\dot{\beta} \qquad \text{pitch} \qquad (19)$$

$$\Delta\dot{h}_z = -A\left(\frac{Hp}{Hr} + \tan\Psi_c\right)(\cos\Psi_c)^2 - C\frac{\dot{H}p}{Hr} \qquad \text{yaw} \qquad (20)$$

The momentum bias on the wheels can be represented in the same manner as it was for the equations of motion.

At this point linearization is accomplished by setting values for constants and zeroing other constants depending on what point we are linearizing about (i.e., at $\beta=90°$, $\Psi=0°$, $h_{yo}=0$, $\Delta h_x=0$). All six equations, three equations of motion and three control equations, are linearized to eliminate all higher order terms. They are represented below having been transformed into the s-plane.

$$0 = I_x \alpha s^2 + \Delta h_x s - \psi h_{yo} s \quad (21a)$$

$$0 = I_y \beta s^2 + \Delta h_y s + \psi h_{xo} s \quad (21b)$$

$$0 = I_z \psi s^2 + \Delta h_z s + \alpha h_{yo} s - \beta h_{xo} s \quad (21c)$$

$$0 = \Delta h_x s - RKp \alpha - RKr \alpha s \quad (21d)$$

$$0 = \Delta h_y s - Kp (\beta - \beta_c) - Kr \beta s \quad (21e)$$

$$0 = \Delta h_z h_{xo} s + A h_{yo} (\cos \Psi_c)^2 + A \Delta h_y (\cos \Psi_c)^2 + A h_{xo} \tan \Psi_c (\cos \Psi_c)^2 + A \Delta h_x \tan \Psi_c (\cos \Psi_c)^2 + C \Delta h_y s \quad (21f)$$

Developing the control equations for $\beta \neq 90°$ differs from the $\beta = 90°$ case because the body coordinates are no longer aligned with the control coordinates, and transformations between the two coordinate systems must be taken into account. The control laws are discussed with the necessary coordinate transformations in the previous section. The final control torques are equations 9-11. The equations of motion, equations 21a-c, remain the same, and the steps for linearization of the control laws do not change with the new equations. The resulting control equations for roll, pitch, and yaw become

$$0 = \Delta h_r s |h_{rd}| \sin \beta + \Delta h_r s |h_{yd}| \cos \beta - \alpha (\sin \beta)^2 |h_{rd}| (RKp + RKr s) - A \tan \Psi_c (\cos \Psi_c)^2 (\cos \beta)^2 \Delta h_y \frac{I_y}{I_r} - C \cos \beta \Delta h_p s \frac{I_y}{I_r} - A \tan \Psi_c (\cos \Psi_c)^2 (\cos \beta)^2 \Delta h_y \frac{I_y}{I_r} - C \cos \beta \Delta h_p s \frac{I_y}{I_r} \quad (22a)$$

$$0 = \Delta h_p s - Kp(\beta - \beta_c) - Kr \beta s \quad (22b)$$

$$0 = \Delta h_y s |h_{rd}| \sin \beta + \Delta h_y s |h_{yd}| \cos \beta - \alpha \cos \beta (RKp + RKr s) |h_{rd}| \sin \beta - \alpha (\cos \beta)^2 (RKp + RKr s) |h_{yd}| + A \sin \beta (\cos \Psi_c)^2 \Delta h_p + A \Delta h_r \tan \Psi_c (\sin \beta)^2 (\cos \Psi_c)^2 + A \Delta h_y \sin \beta \cos \beta (\cos \Psi_c)^2 + C \sin \beta \Delta h_p s \quad (22c)$$

Using the linearized equations, root locus plots were made for several different combinations of beta and psi angles and different parameters (Kp, Kr, A, C, Kp and Kr, and A and C, [see figure 6]). From the root locus plots it is possible to determine the stability margins for the linearized system. These stability margins were used to help find acceptable operating gain margins for the entire non-linear system.

The numerical analysis was done using the Interactive

Controls Analysis (INCA) software package. From the plots it was possible to determine the gains that would drive the system unstable (see "boundary crossings" on plots). Appendix D contains root locus plots for the nominal operation points as well as the points where instability occurs.

B. Simulations

The gain margins found using the root locus plots represent the instability points for the linearized system. To find acceptable operating points for the system, a computer simulation was written to simulate the actual responses of the satellite to different commanded angles with the zero-gyro control laws.

Using the simulation it was possible to test the margins found in the root locus analysis, examine performance and settling time, adjust the margins slightly and reexamine the results several times.

Appendix E contains plots generated with data from the simulation. The data included has plots for nominal operating points as well as instability points. It begins with the linear case and non-linearities (including reaction wheel torque limits, computer sampling, wheel tachometer quantization, D/A converter quantization) are gradually added. Table 1 compares the instability points found using the root locus plots with the instability points found in the simulation. For the simulation, results are given for both the linear and complete non-linear cases.

The simulation is organized into four main parts. It models a dynamic simulator, attitude sensors, an on-board computer, and reaction wheels. The sensors take information about wheel and body momentum from the dynamic simulator and determine the attitude of the spacecraft in terms of the roll, pitch, and yaw angles. The current attitude and the commanded attitude are fed into the on-board computer. The computer uses this information and the control laws to compute the control torque and command voltage for the reaction wheels. The reaction wheel model receives a voltage from the computer and accelerates the proper amount. The dynamic simulator is responsible for integrating the equations of motion,

determining the motion of the body, and converting this to the attitude sensor information, which in turn feeds the control law.

IV. **Results and Conclusions**

For the case where β=90 degrees, the linear analysis and simulation stability points compare favorably, and in some cases the addition of non-linearities actually gives the system more gain margin. The linear version of the simulation eliminates as many non-linearities as possible; however, it was not possible to create a completely linear simulation. This may account for some of the discrepancies between the root locus and linear simulation gain margins. From this analysis it appears that the control laws for β=90° may be able to provide fine error sensor target capture for the IUE satellite. Table 1 gives the stability points for the root locus, linear and non-linear simulations of the β=90° control laws.

Linear analysis has been completed for quadrant I only of the $\beta\neq$90° control laws. Linear simulations done for this operating range have compared favorably with the linear analysis. Operation of the $\beta\neq$90° control law in the range where β is 90 degrees also compares

Table 1
Gain Margins Found with Root Locus and Simulations
for the β=90° Control Laws

Parameter	Angle Psi degrees	Root Locus dB	Low Fidelity Simulation Linear dB	Non-linear dB
Kp	+/- 45	-23.35	<-30	
Kr	+/- 45	-15.92	-15.9	
A	+/- 45	20.79	21.9	
C	+/- 45	22.54	22.6	
Kt*	0	-25.73	<-30	
Pitch loop	0,+/- 45	-26.28	<-30	-26
Yaw loop	0,+/- 45	19.71	17.7	22.9

(note: the pitch parameters have a lower gain margin; yaw parameters have an upper gain margin)

favorably to the results of the $\beta=90°$ control laws. However, problems do exist. The full operational range of the IUE satellite is not stable with nominal gains chosen for the $\beta\neq90°$ control law. These gains will be changed based on the root locus plots and the whole process will be iterated until the entire operational envelope is stable. Table 2 shows the stability points of the root locus, linear and non-linear simulations for the $\beta\neq90°$ control laws as well as regions where nominal stability does not exist. For the regions where nominal stability does not exist, fine adjustment of the gains will be necessary to produce operational stability. Some of the numbers in Table 2 do not represent complete instability; however, the settling time at this point is so large that it would not be practical.

Table 2
Gain Margins Found with Root Locus and Simulations
for the $\beta=90$ Control Laws
using Nominal $\beta=90$ Gains

			Low Fidelity Simulation	
Angles degrees	Pitch or Yaw	Root Locus dB	Linear dB	Non-linear dB
$\beta=90,\Psi=0$	Pitch	-20.87	-20	<-30
	Yaw	21.03	13.44	19.0
$\beta=90,\Psi=44$	Pitch	-21.03	-20	<-30
	Yaw	20.50	19.55	22.28*
$\beta=90,\Psi=-44$	Pitch	-21.25	-20	<-30
	Yaw	20.50	19.55	22.28*
$\beta=45,\Psi=0$	Pitch	-22.53	-20	<-30
	Yaw	21.04	13.62	9.54
$\beta=45,\Psi=44$	Pitch	Unstable using $\beta=90$ Gains		
	Yaw	Unstable using $\beta=90$ Gains		
$\beta=45,\Psi=-44$	Pitch	Unstable using $\beta=90$ Gains		
	Yaw	Unstable using $\beta=90$ Gains		

*Values where system is stable, but settling time is very large.

Currently, analysis and simulations are in progress to achieve global stability of the IUE zero-gyro control system. Full non-linear simulations of all operational scenarios will follow and will be documented in another technical memorandum.

The authors would like to credit Henry Hoffman and Dr. Thomas Flatley of the Guidance and Control Branch of the NASA Goddard Space Flight Center (GSFC) with the development of the zero-gyro concept. Credit also goes to Mr. James Donohue, also at NASA GSFC for the beginning linear analysis and gain selection work which provided the foundation on which this paper is based. Technical consultants included Mike Femiano (GSFC), Dr. Thomas Flatley, Henry Hoffman, and several Bendix employees at the IUEOCC at GSFC.

Appendix A
Symbolic Block Diagram for Yaw Axis Control Law

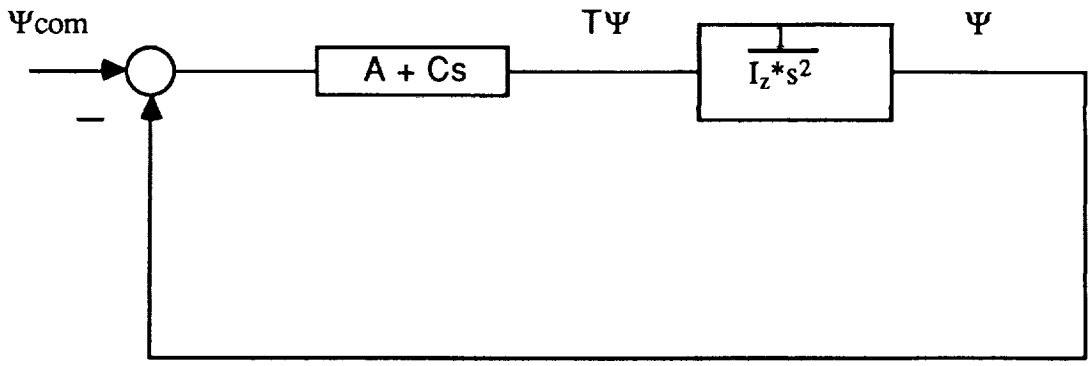

$$T_\Psi = A(\Psi_{com} - \Psi) - C\dot{\Psi}$$

wheel torque = - spacecraft torque

$$T_w = A(\Psi - \Psi_{com}) + C\dot{\Psi}$$

where

T_Ψ = torque exerted by the reaction wheel onto the spacecraft

T_w = torque command to reaction wheel

Appendix B
Small Angle Approximations for the Yaw Control Law

The yaw control law was simplified using some trigonometric identities and small angle approximations. In order to prove the validity of the simplifications, it is necessary to show that

$$\arctan\left(\frac{-Hp}{Hr}\right) - \Psi_{com} \cong -(\cos\Psi_{com})^2\left(\frac{Hp}{Hr} + \tan\Psi_{com}\right).$$

After taking the tangent of both sides the following identity is helpful

$$\tan x \pm y = \frac{\tan x \pm \tan y}{1 \ \tan x \tan y}.$$

Expanding the equation will give

$$\frac{-\frac{Hp}{Hr} - \tan\Psi_{com}}{1 - \frac{Hp}{Hr}\tan\Psi_{com}} = \tan\left(-\left(\cos\left(\frac{Hp}{Hr} + \tan\Psi_{com}\right)\right)^2\right)$$

Using the small angle approximation tan x = x on the right-hand side of the equation we are left with

$$\frac{-1\left(\frac{Hp}{Hr} + \tan\Psi_{com}\right)}{1 - \frac{Hp}{Hr}\tan\Psi_{com}} = -\left(\cos\left(\frac{Hp}{Hr} + \tan\Psi_{com}\right)\right)^2.$$

The term $-1\left(\frac{Hp}{Hr} + \tan\Psi_{com}\right)$ will cancel from both sides and the remaining expression is

$$\frac{1}{1 - \frac{Hp}{Hr}\tan\Psi_{com}} = (\cos\Psi_{com})^2.$$

From here, cross multiplication and the substitution of

$$\tan\Psi_{com} = \frac{\sin\Psi_{com}}{\cos\Psi_{com}} \quad \text{and} \quad \tan\Psi_{com} = -\frac{Hp}{Hr}$$

will yield

$$(\cos \Psi_{com})^2 + (\sin \Psi_{com})^2 = 1 \ .$$

Therefore the simplifications made in the yaw control law from equation 5 to equation 6 are valid.

Appendix C

Control Constants

Axis	Bandwidth (rad/sec)	Damping
p x s	0.2	0.076
pitch	0.2	0.076
sunline	0.015	0.076

SPACECRAFT CONTROL CONSTANTS

Ix = 109.3 slug-ft^2

Iy = 211.5 slug-ft^2

Iz = 242.9 slug-ft^2

Kt = reaction wheel torque constant = 0.012 ft-lb/volt

+/- 2.5 volts full scale

τ = reaction wheel time constant = 640 seconds

hro = initial roll wheel momentum for beta=90 degrees, psi=0 degrees in linear analysis model = 0.26 ft-lb-sec

CONTINUED ON NEXT PAGE

Conversion from Control Frame Computed Torque to Acceleration:

let $[I_b]$ = body frame inertias ; $[I_c]$ = inertias represented in control frame ;

$[R]$ = body frame to control frame transformation ; $[R]^T$ = control frame to body frame transformation ; T_c = computed torque in control frame ;

$\overline{\alpha_c}$ = control frame acceleration ; $\overline{\alpha_b}$ = body frame acceleration

PROOF :

$\overline{\alpha_c} = ([I_c]^{-1})T_c \rightarrow \overline{\alpha_c} = (([R][I_b][R]^T)^{-1})T_c \rightarrow \overline{\alpha_b} = [R]^T \overline{\alpha_c} \rightarrow$

$\overline{\alpha_b} = [R]^T(([R]^T)^{-1}([I_b])^{-1}([R])^{-1})T_c \rightarrow \overline{\alpha_b} = ([R]^T[R][I_b]^{-1}[R]^T)T_c \rightarrow$

$\overline{\alpha_b} = ([I_b]^{-1}[R]^T)T_c \rightarrow \overline{\alpha_c} = ([I_b]^{-1})T_c$ assuming no products of inertia

Therefore, acceleration in the control frame can be computed by taking the torque computed in the control frame and dividing by the body inertias.

Appendix D
Root Locus Plots

The following pages contain root locus plots for the linear analysis of both the $\beta=90$ and $\beta\neq90$ control laws with psi angles of 0 and 45 degrees. Included are root loci of the pitch and yaw loop gains. The plots include root loci for the following control laws and angles:

		β (deg)	Ψ (deg)
D1	$\beta=90$ control law pitch loop	90	0
D2	$\beta=90$ control law yaw loop	90	0
D3	$\beta=90$ control law pitch loop	90	45
D4	$\beta=90$ control law yaw loop	90	45
D5	$\beta\neq90$ control law pitch loop	90	0
D6	$\beta\neq90$ control law pitch loop	90	45
D7	$\beta\neq90$ control law pitch loop	45	0
D8	$\beta\neq90$ control law yaw loop	90	0
D9	$\beta\neq90$ control law yaw loop	90	45
D10	$\beta\neq90$ control law yaw loop	45	0

The time is 16:40:14.32 25-JAN-1989
Project: IHEA

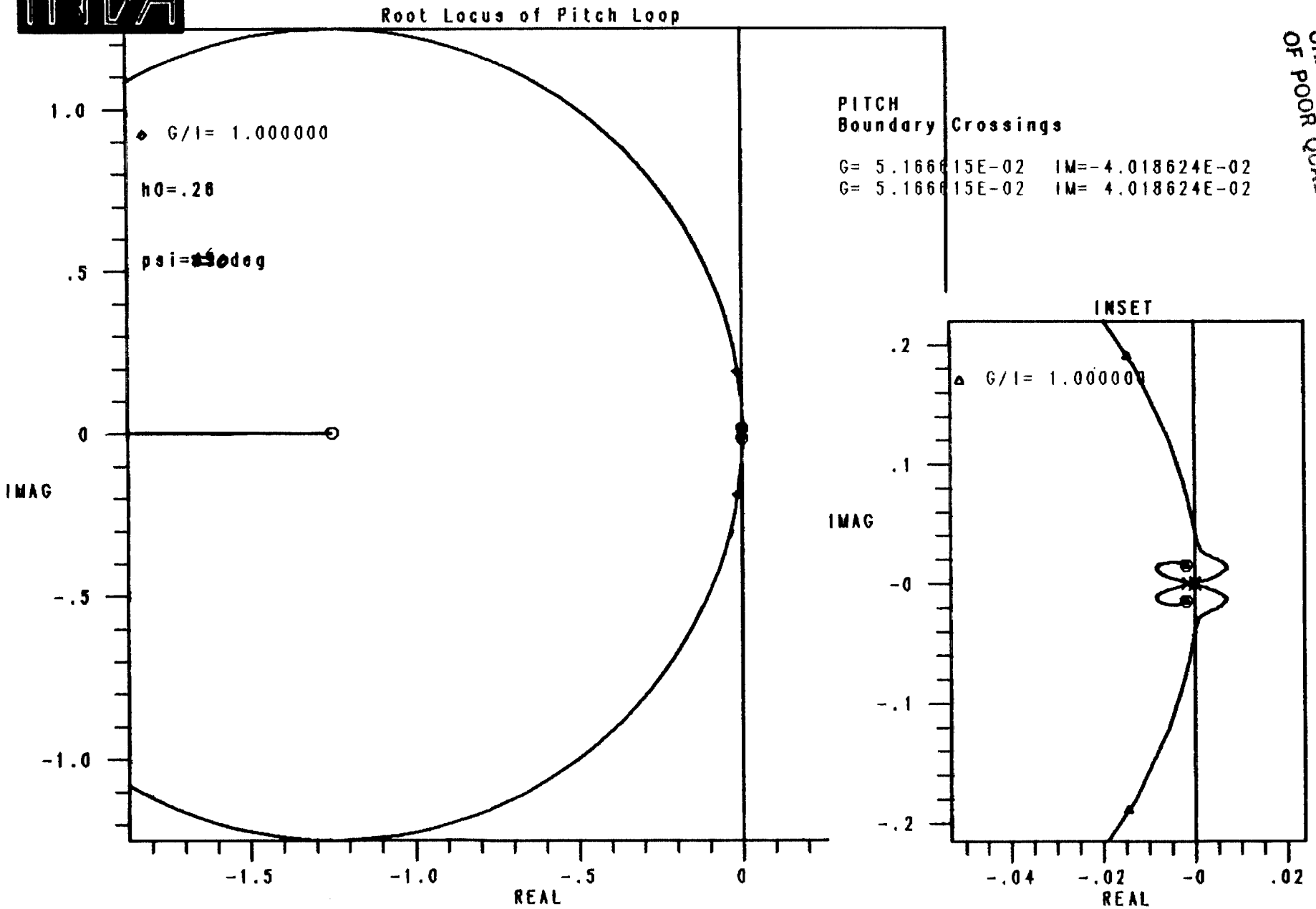

The time is 16:49:37.49 25-JAN-1989
Project: IUEA

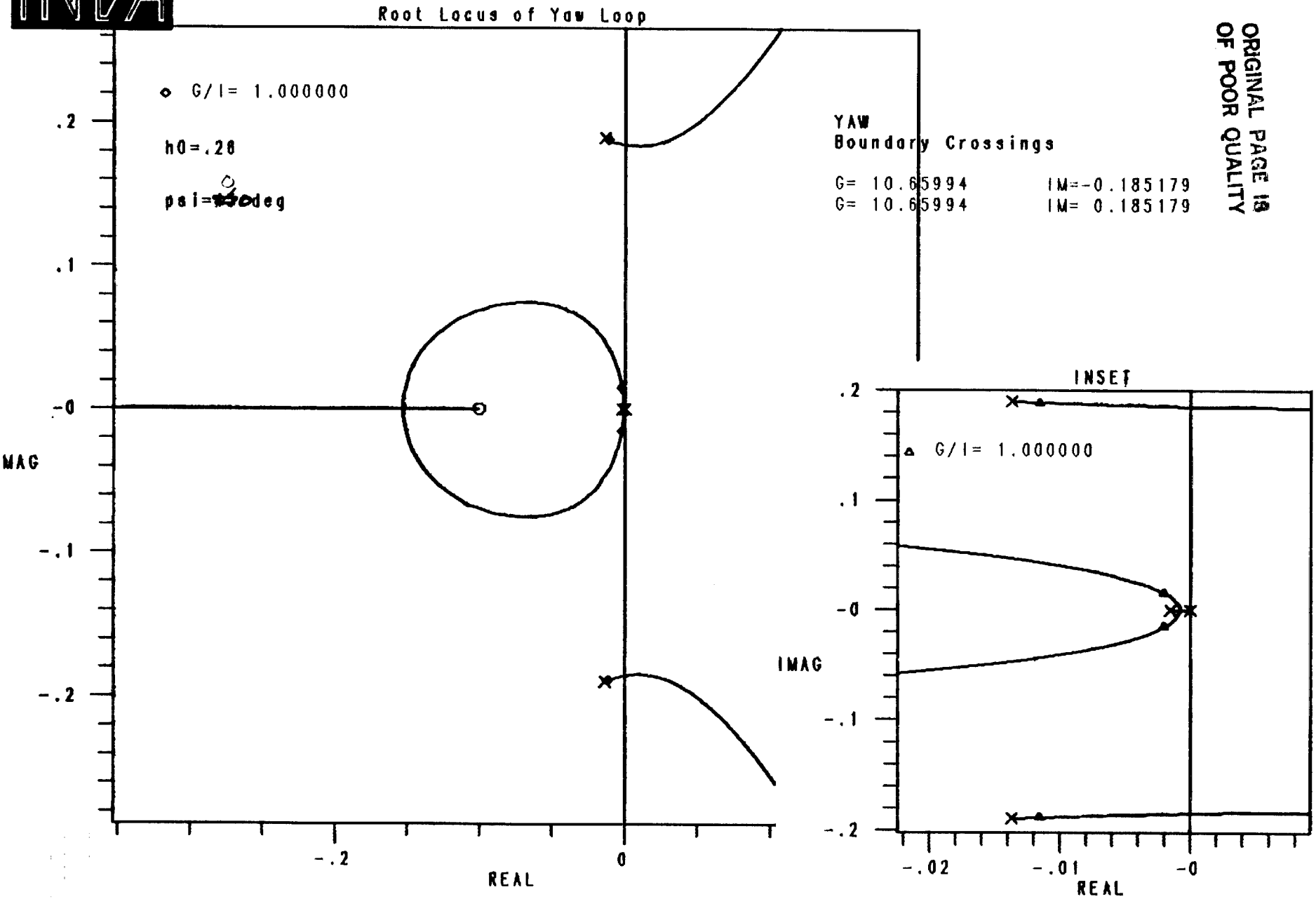

D3

The time is 14:44:54.32 27-JAN-1989
Project: IUEB

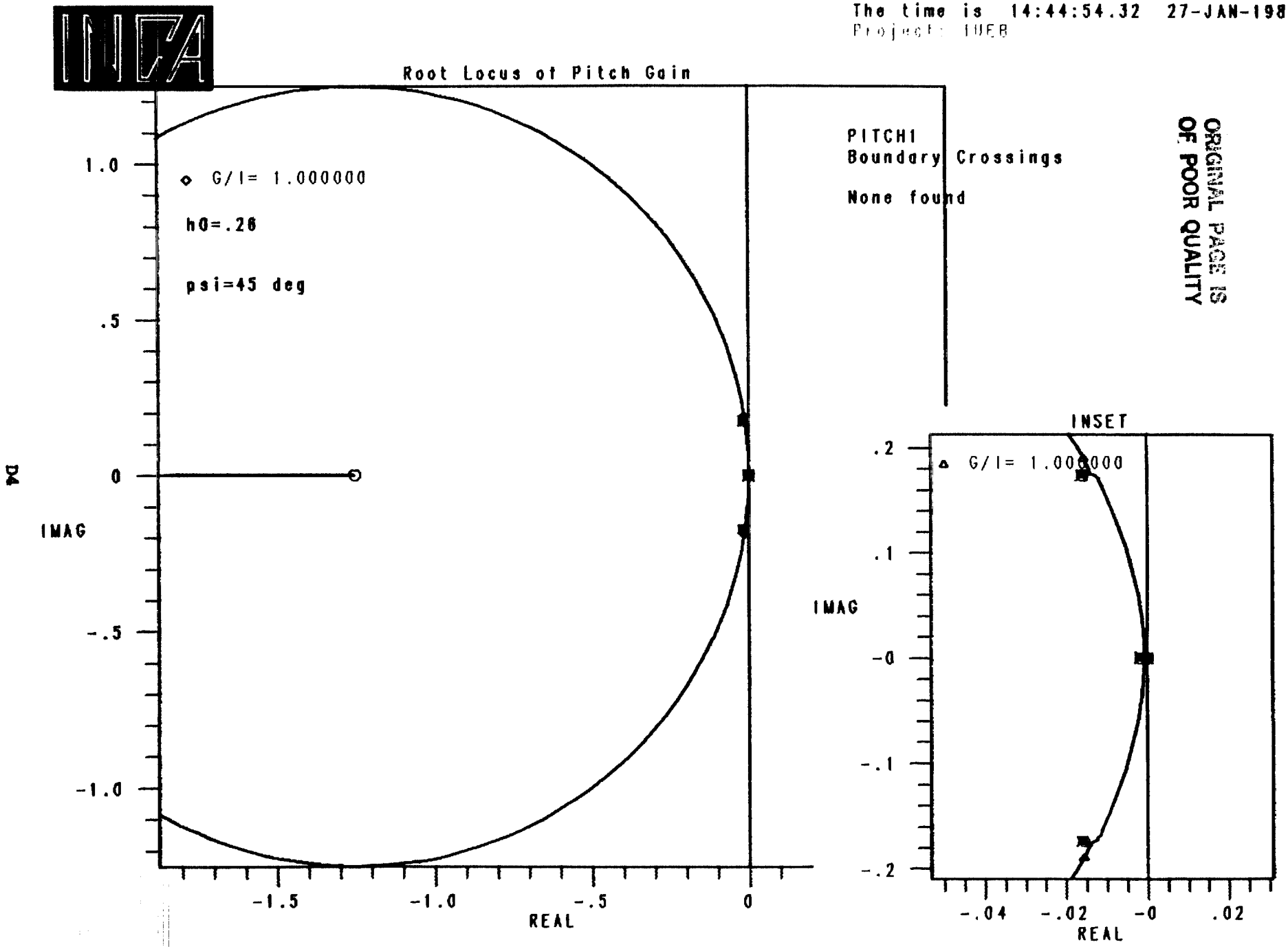

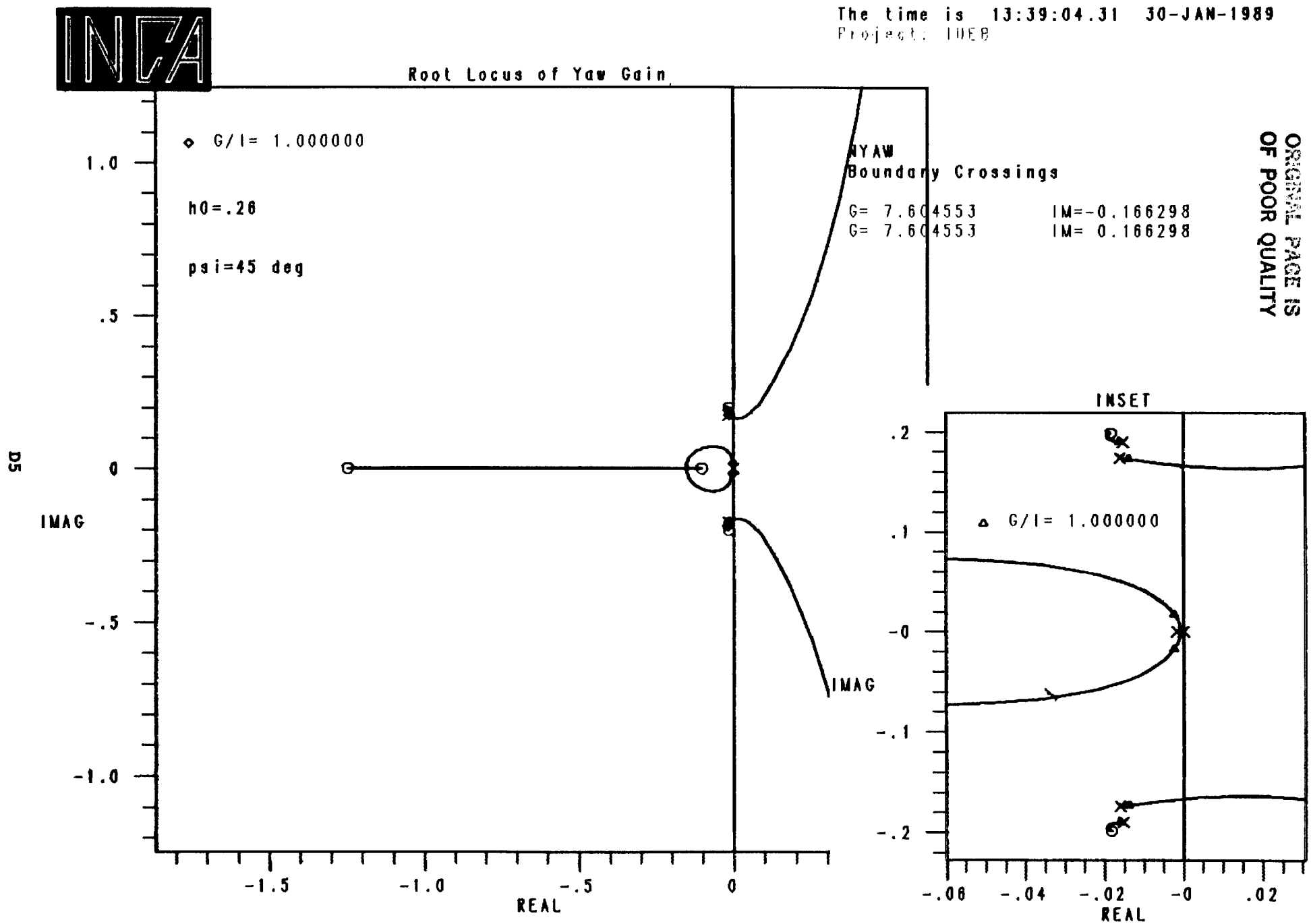
The time is 13:39:04.31 30-JAN-1989
Project: IDEB
Root Locus of Yaw Gain
◇ G/I= 1.000000
h0=.26
psi=45 deg
NYAW
Boundary Crossings
G= 7.604553 IM=-0.166298
G= 7.604553 IM= 0.166298
1.0
.5
0
-.5
-1.0
IMAG
-1.5
-1.0
-.5
0
REAL
INSET
△ G/I= 1.000000
.2
.1
-0
-.1
-.2
IMAG
-.06
-.04
-.02
-0
.02
REAL
ORIGINAL PAGE IS
OF POOR QUALITY
D5

The time is 14:04:40.37 22-JUL-1989
Project: MBETA

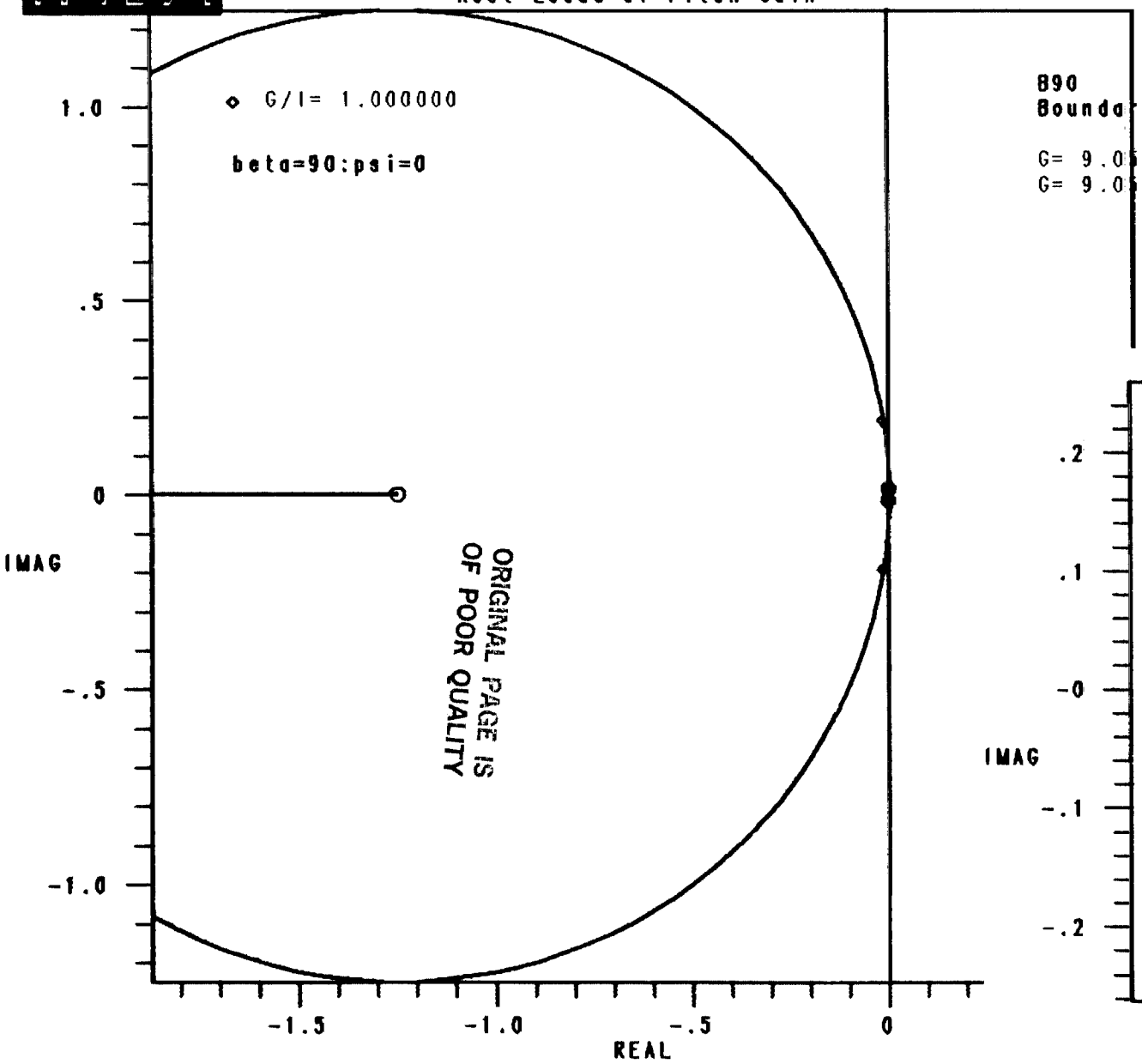

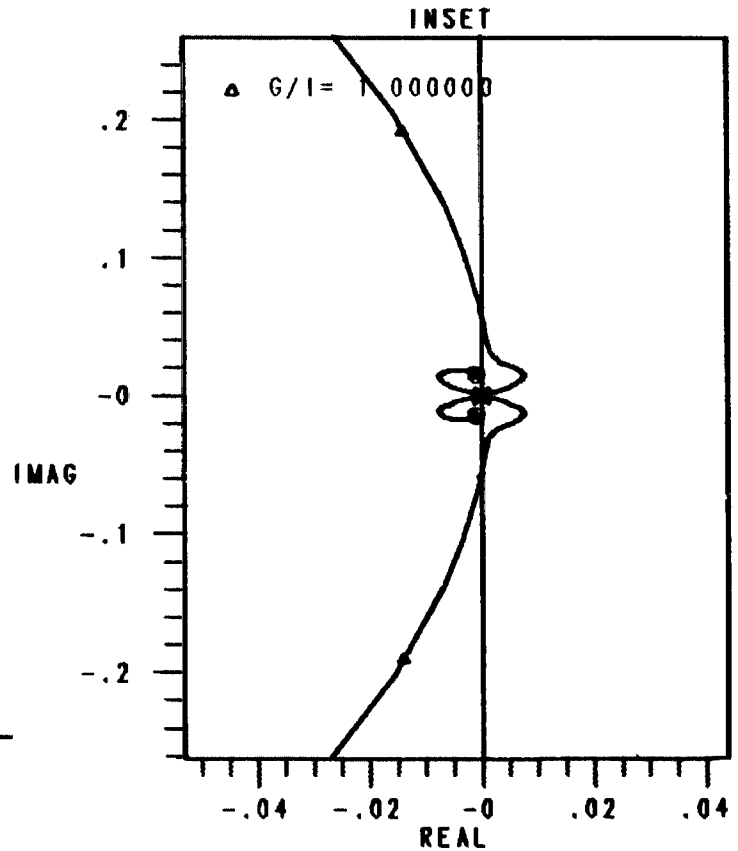

The time is 14:27:37.98 22-JUL-1989
Project: NBETA

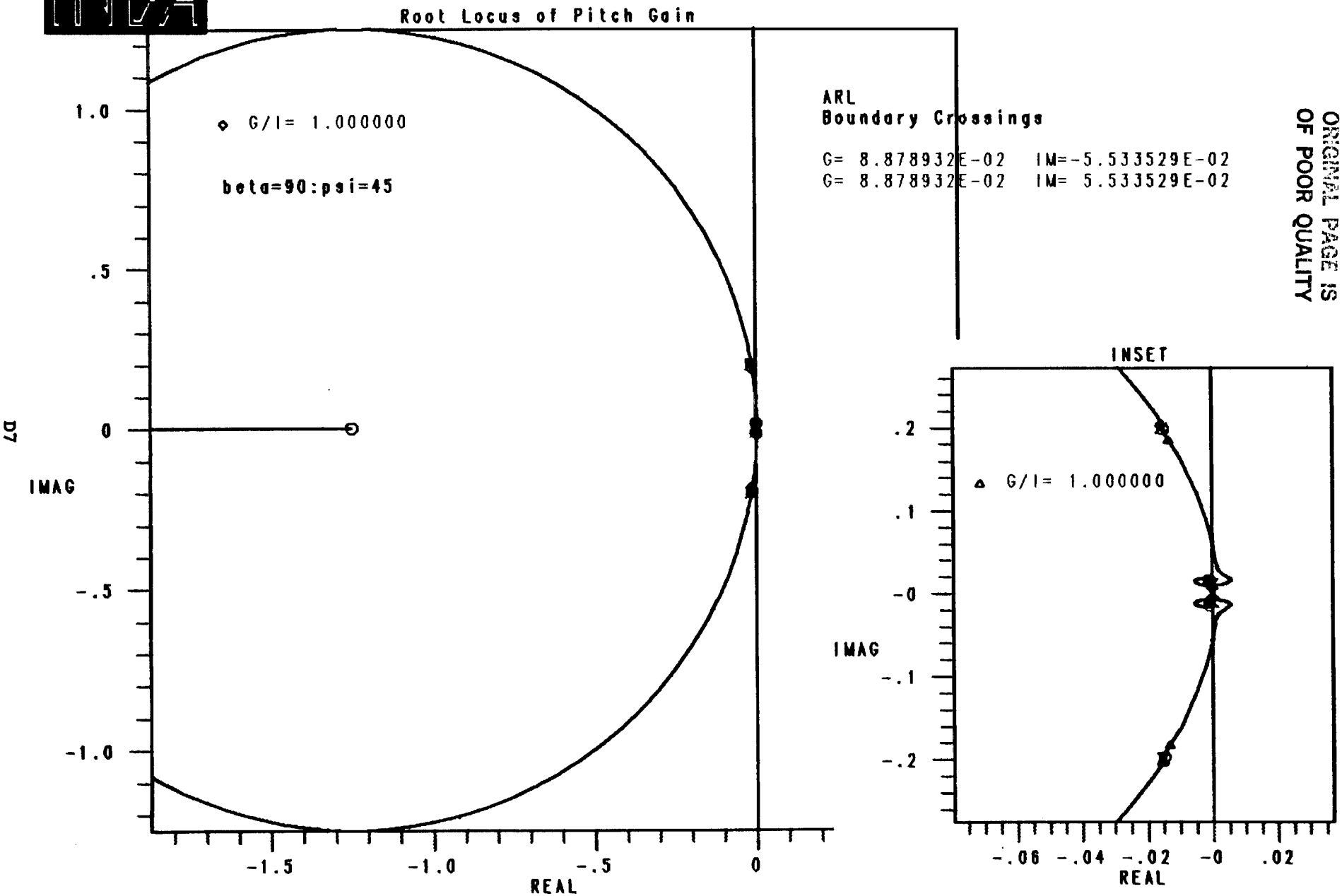

D7

The time is 14:41:28.55 22-JUL-1989
Project: MBCIA

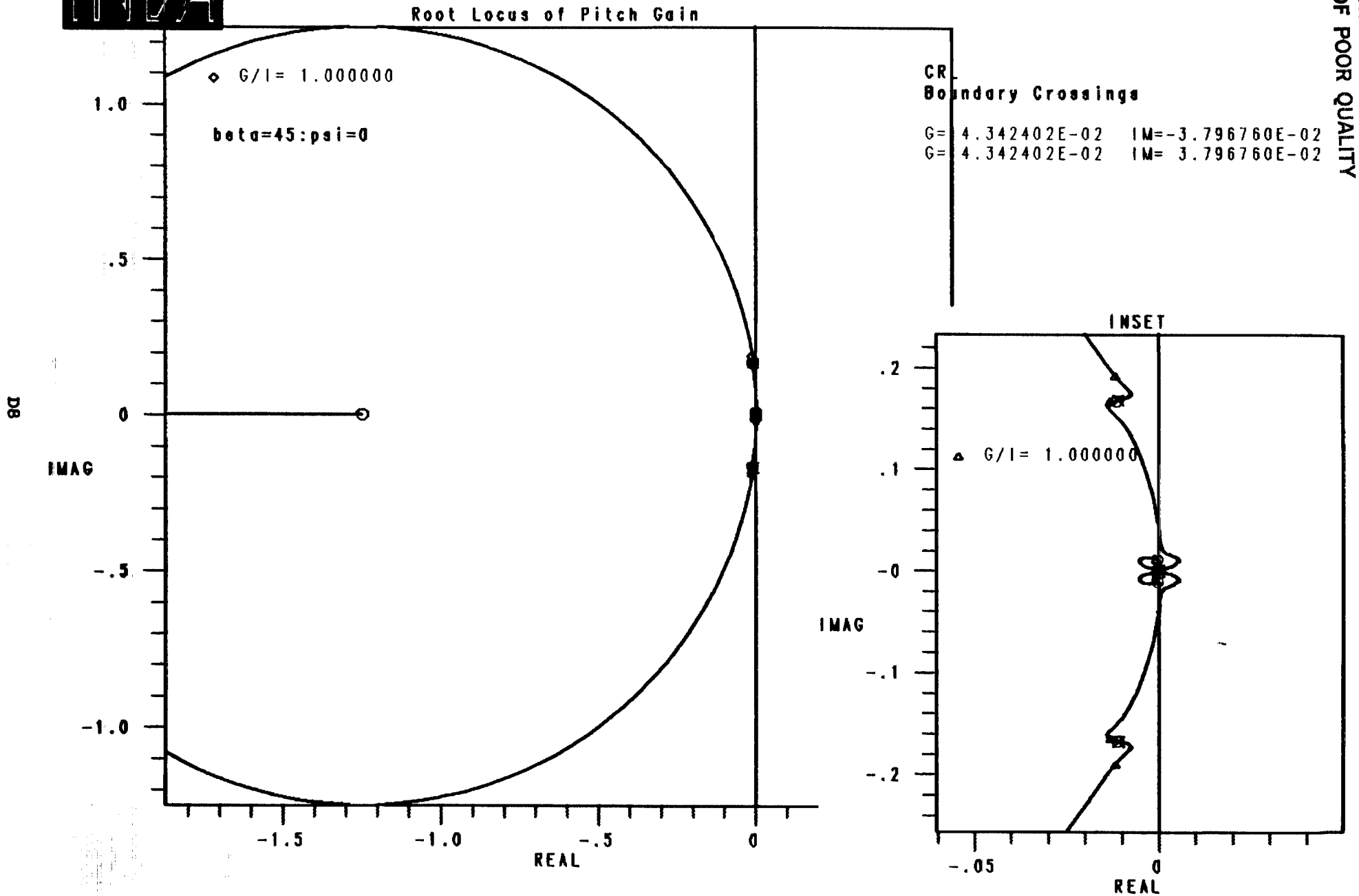

The time is 16:39:02.57 19-JUL-1989
Project: NBETAY

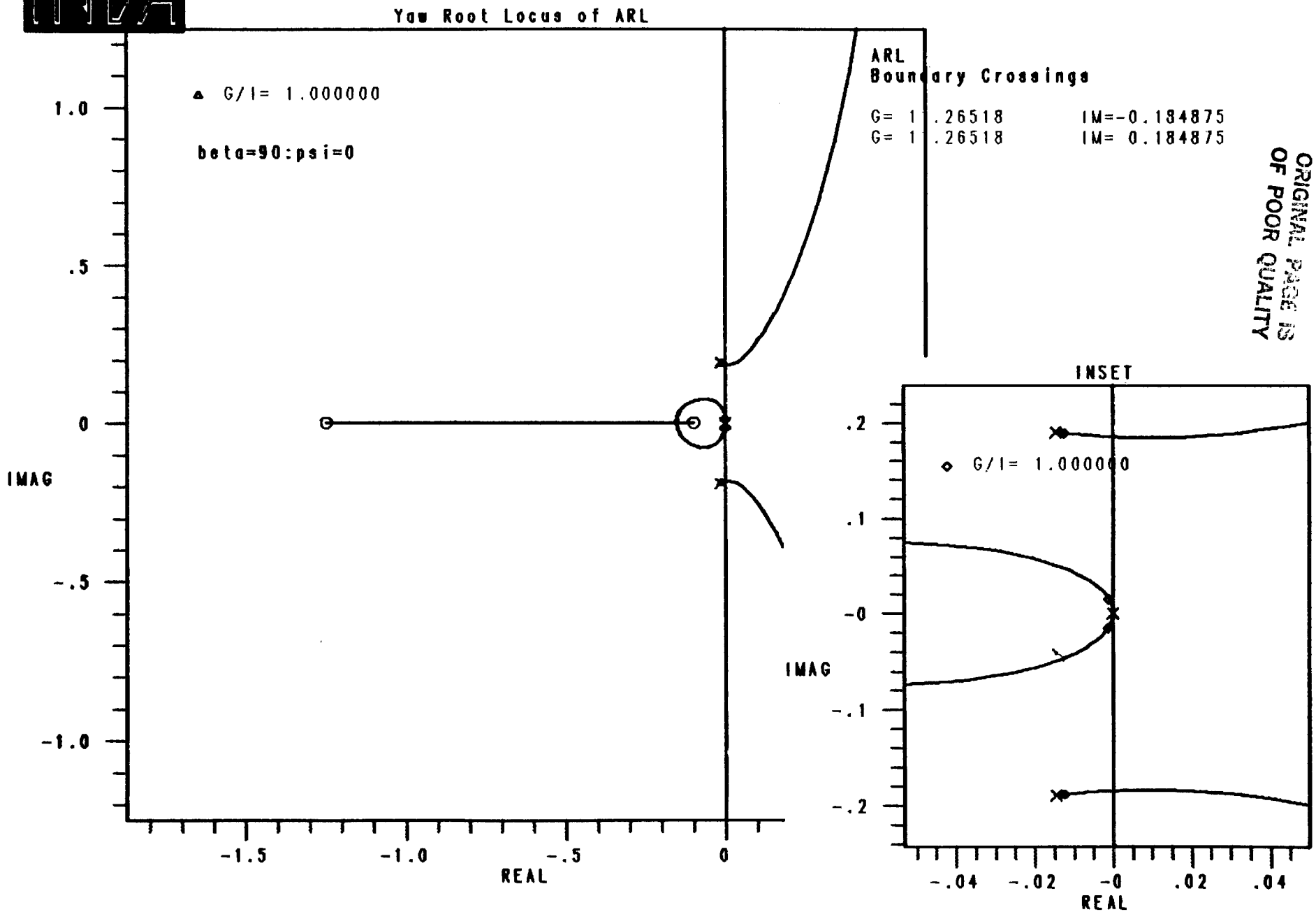

The time is 16:51:35.15 19-JUL-1989
Project: NBETAF

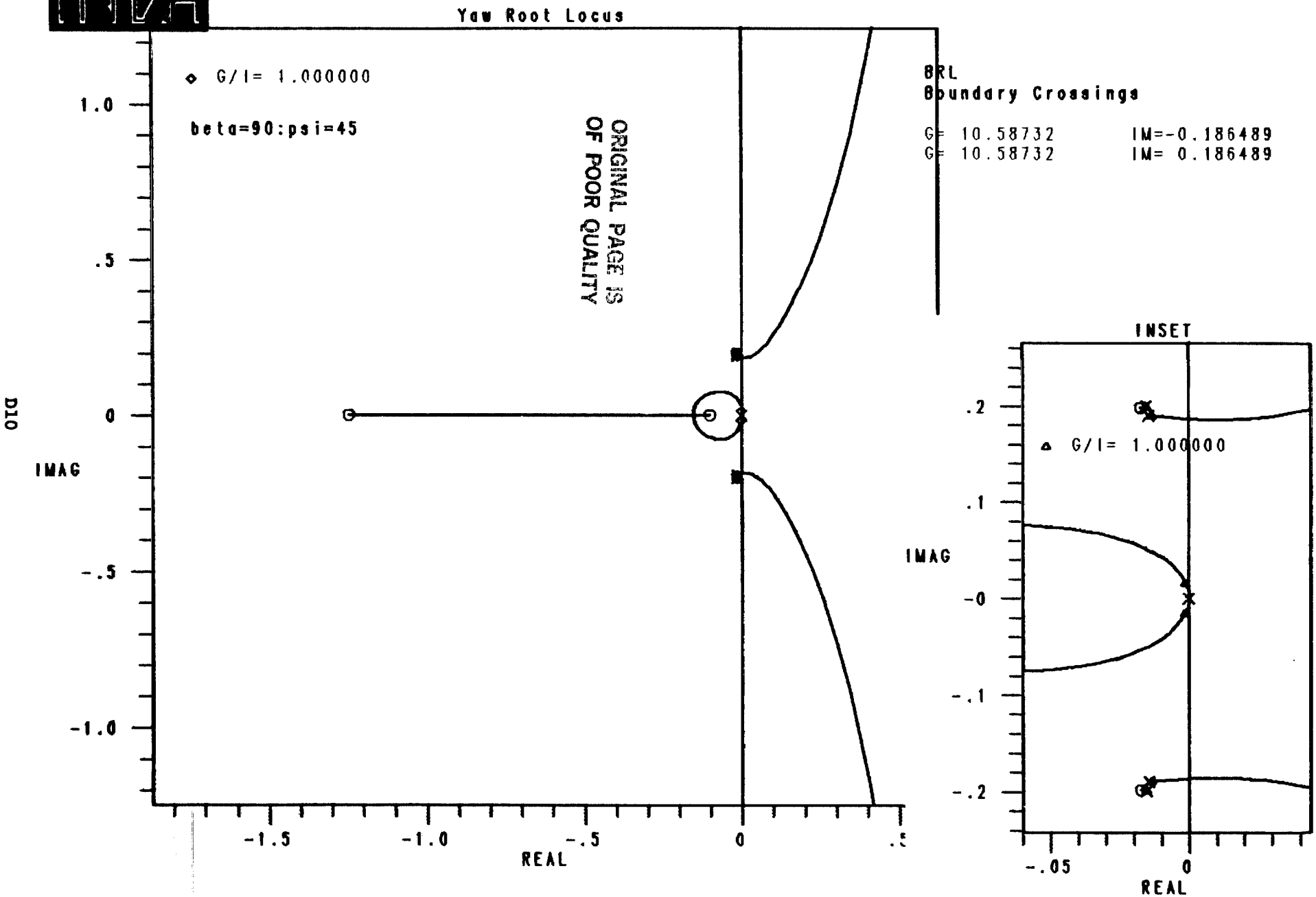

The time is 14:57:23.46 22-JUL-1989
Project: NRETAF

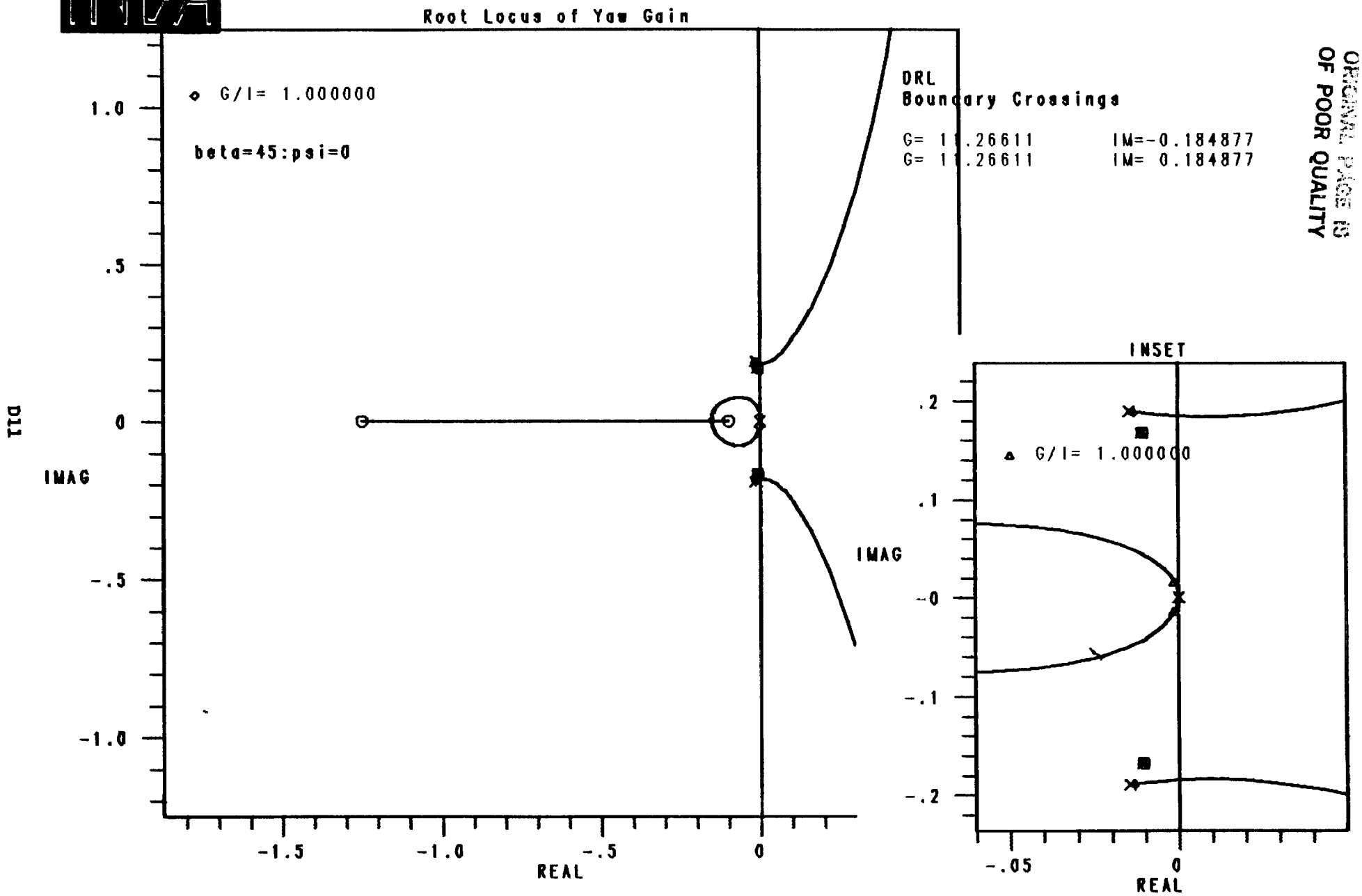

Appendix E
Simulation Plots

The following pages contain plots of the performance of the IUE satellite in response to various slew maneuvers using the zero-gyro control laws as predicted by the low-fidelity simulation. The plots represent the movement of the satellite in terms of its three rotation angles, alpha, beta, and psi. In some cases, the rate of rotation about the sunline is examined instead of the psi angle (this is labelled psi rate) due to the difficulty in computing the actual angle psi within the simulation itself. The plots represent the following control laws and commanded angles:

		β (deg)	Ψ (deg)
E1	β=90 linear control law	91	0
E2	β=90 linear control law	90	44
E3	β=90 non-linear control law	90	5
E4	β=90 non-linear control law	90	44
E5	β≠90 linear control law	91	0
E6	β≠90 linear control law	90	44
E7	β≠90 linear control law	45	0
E8	β≠90 non-linear control law	91	0
E9	β≠90 non-linear control law	90	44
E10	β≠90 non-linear control law	45	0

File: IUEEA.OUT

the time is 14:35:45.88 28-FEB-1988

BETA=0:PSI=0.0;NOMINAL GAINS;TSAMP=0.2

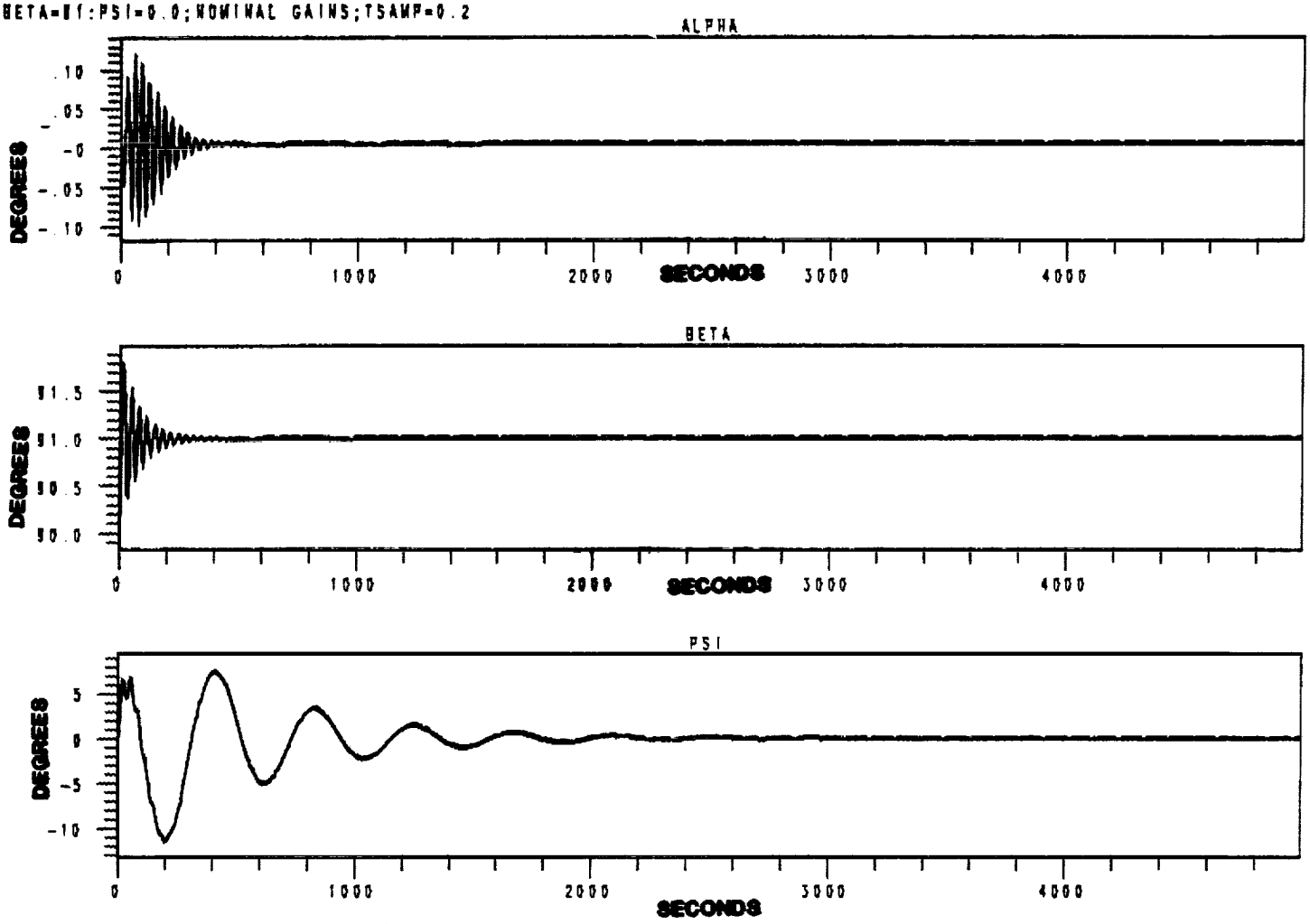

File: IUEEA.OUT

The time is 16:18:58.07 21-FEB-1988

BETA=80;PSI0=44;NOMINAL GAINS

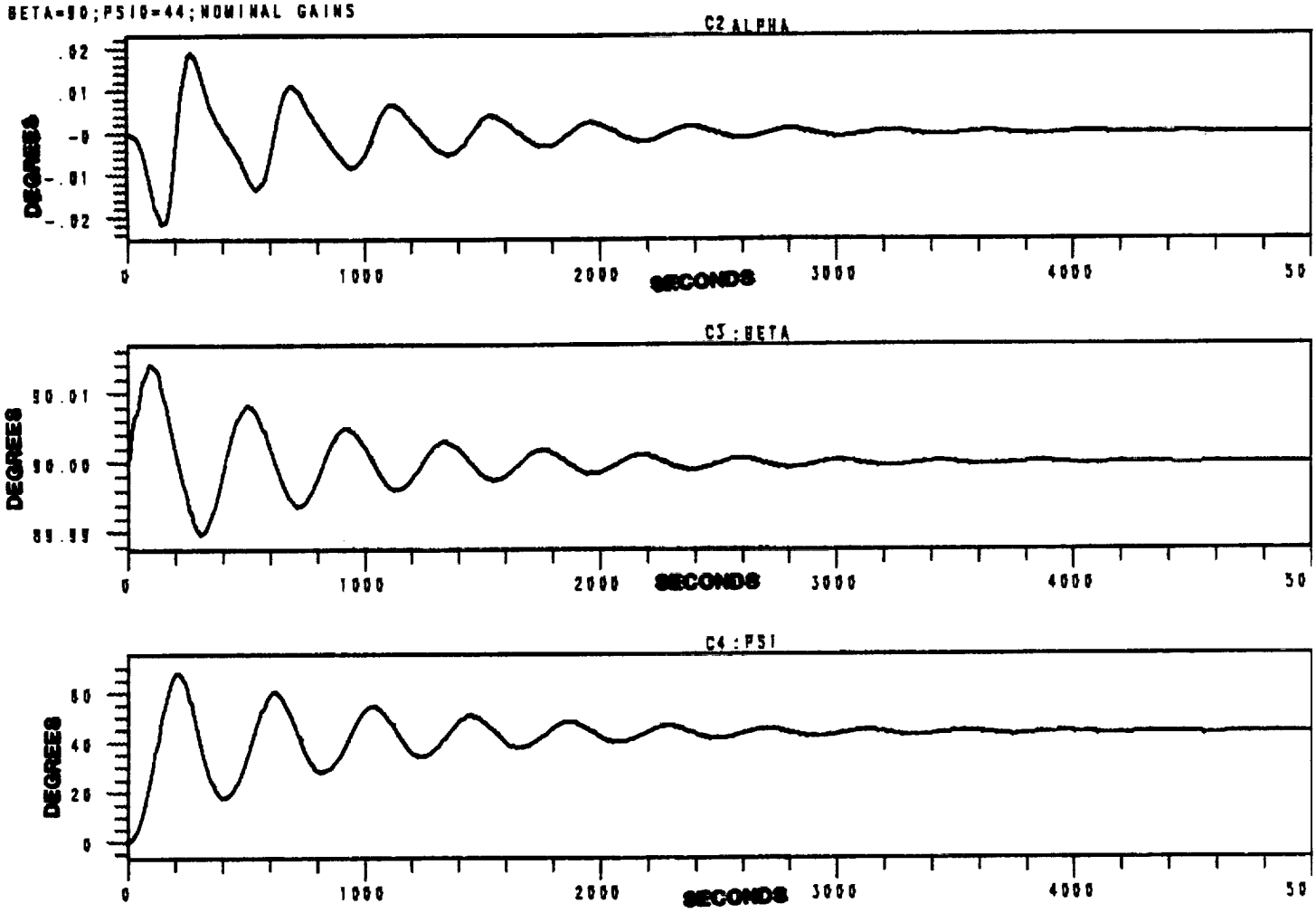

File: IUEEA.OUT

The time is 13:34:23.44. 22-JUL-1989

beta=90:psi=5:nominal gains:nonlinear

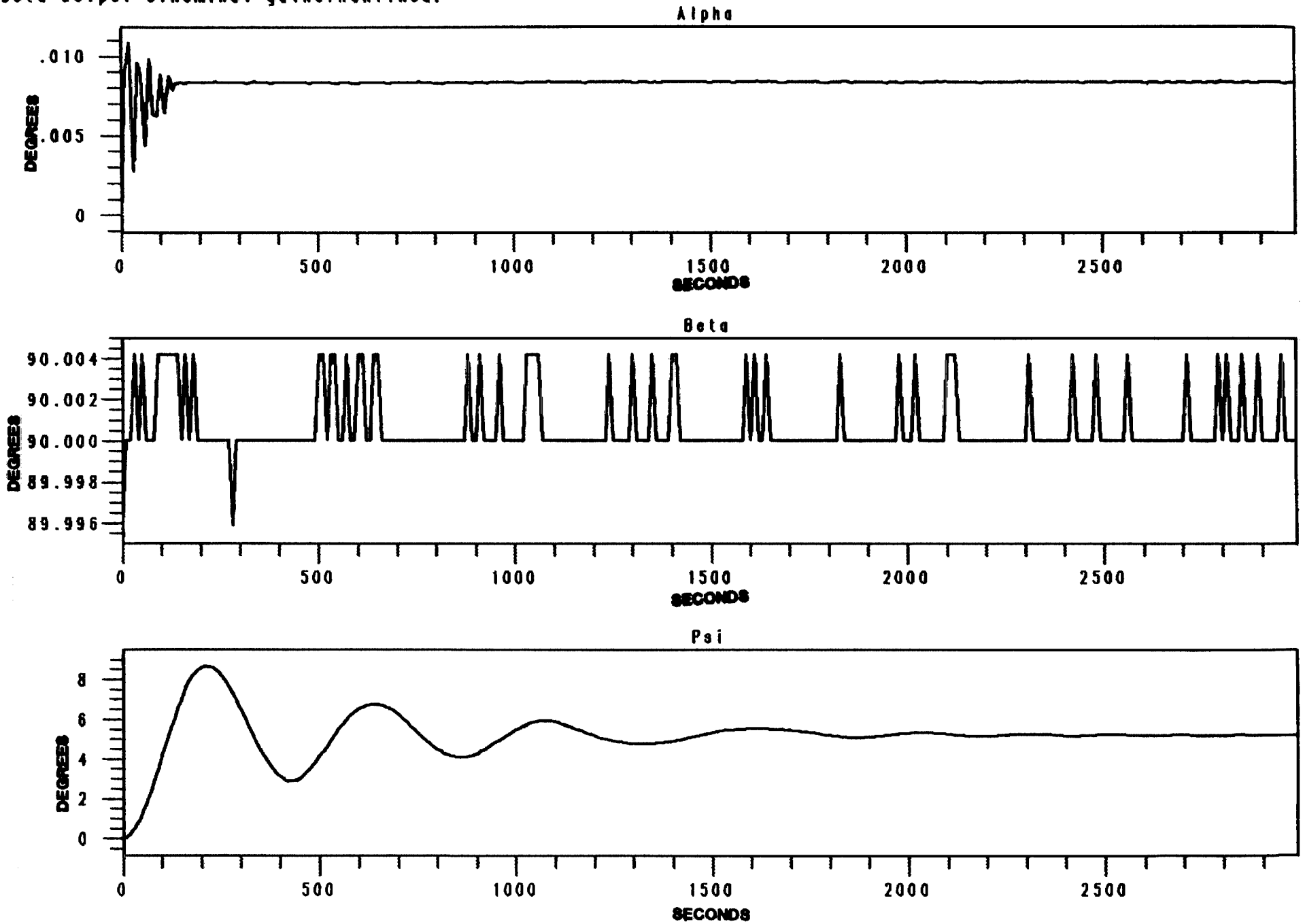

File: IUEEA.OUT

The time is 13:51:33.30 22-JUL-1989

beta=90:psi=44:nominal gains:non-linear

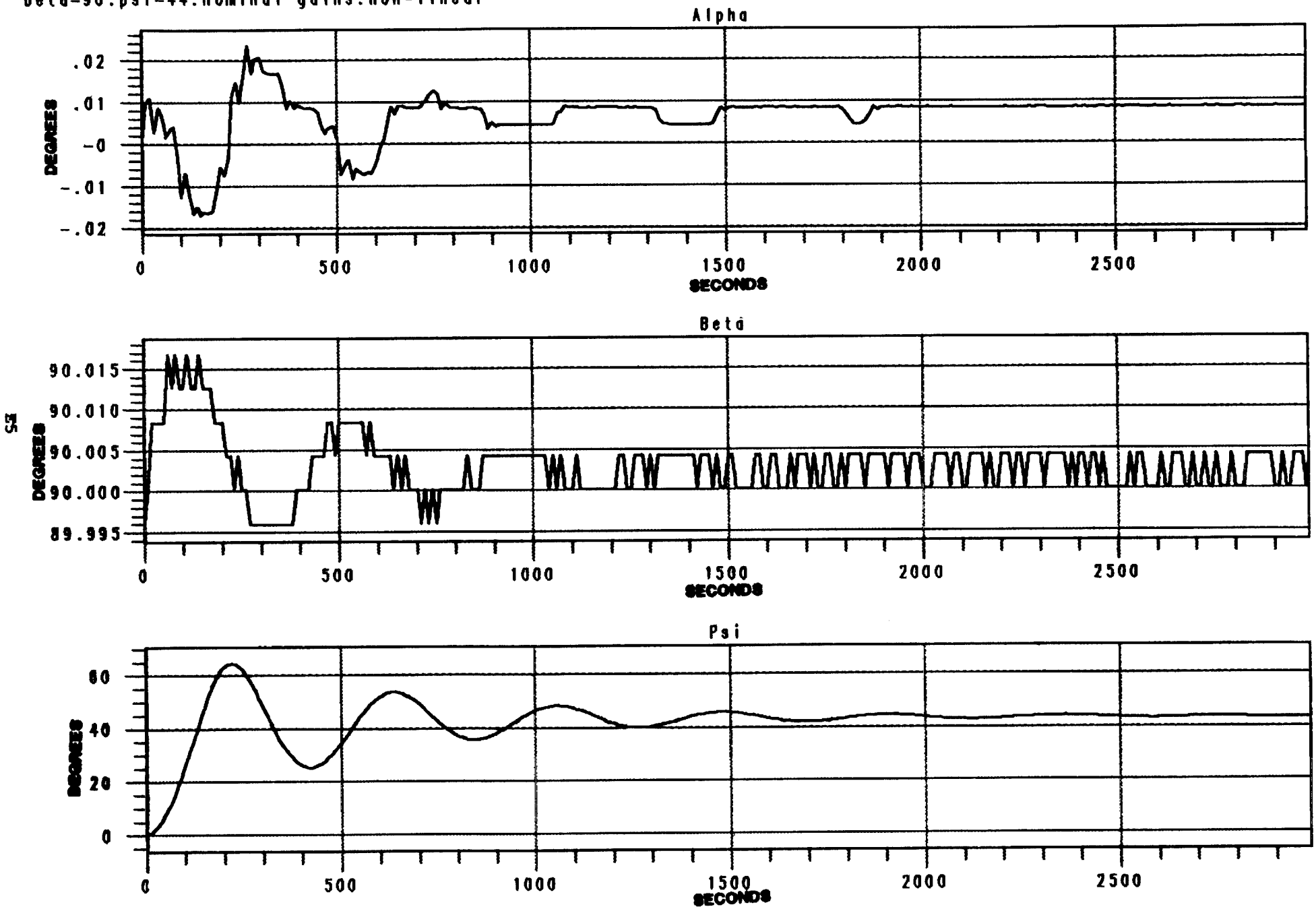

File: IUERN OUT

The time is 15:39:43.02 22-JUL-1989

BETA=91:PSI=0:NOMINAL GAINS:LINEAR

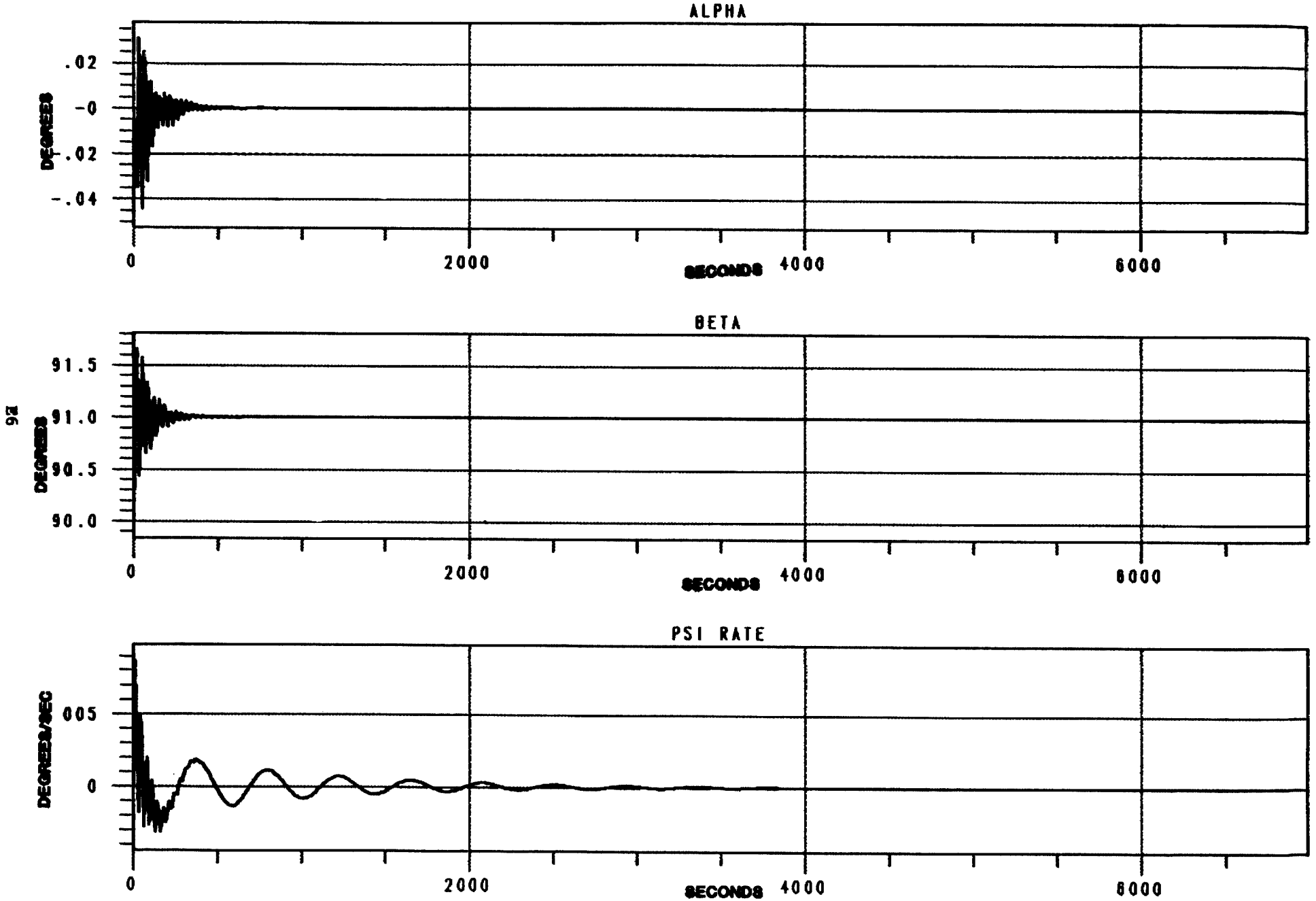

File: IUEBN.OUT

The time is 15:52:22.67 22-JUL-1989

BETA=90:PSI=44:NOMINAL GAINS:LINEAR

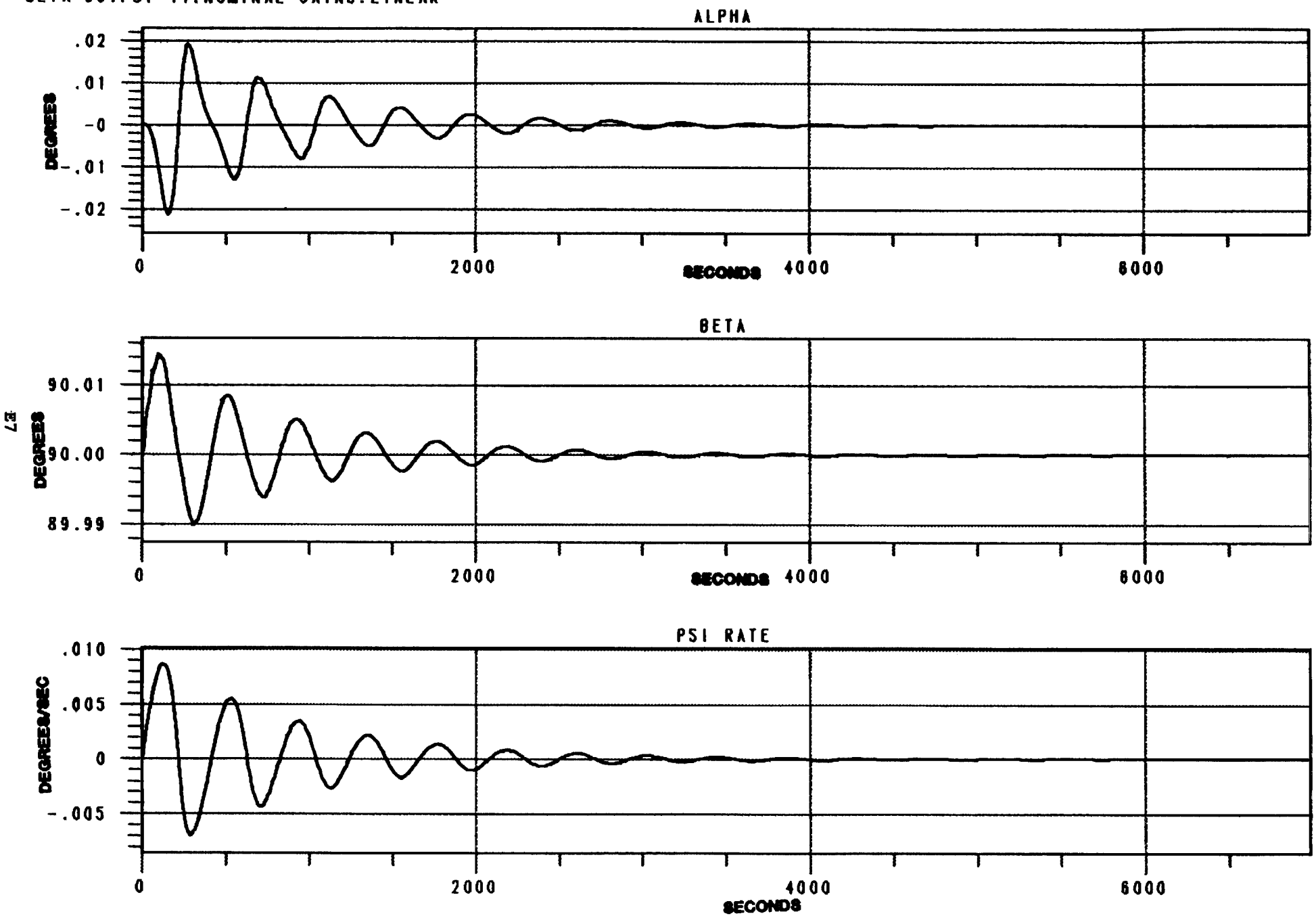

File: IUEBN.OUT

The time is 17:08:34.02 24-JUL-1989

BETA=45:PSI=0:NOMINAL GAINS:LINEAR

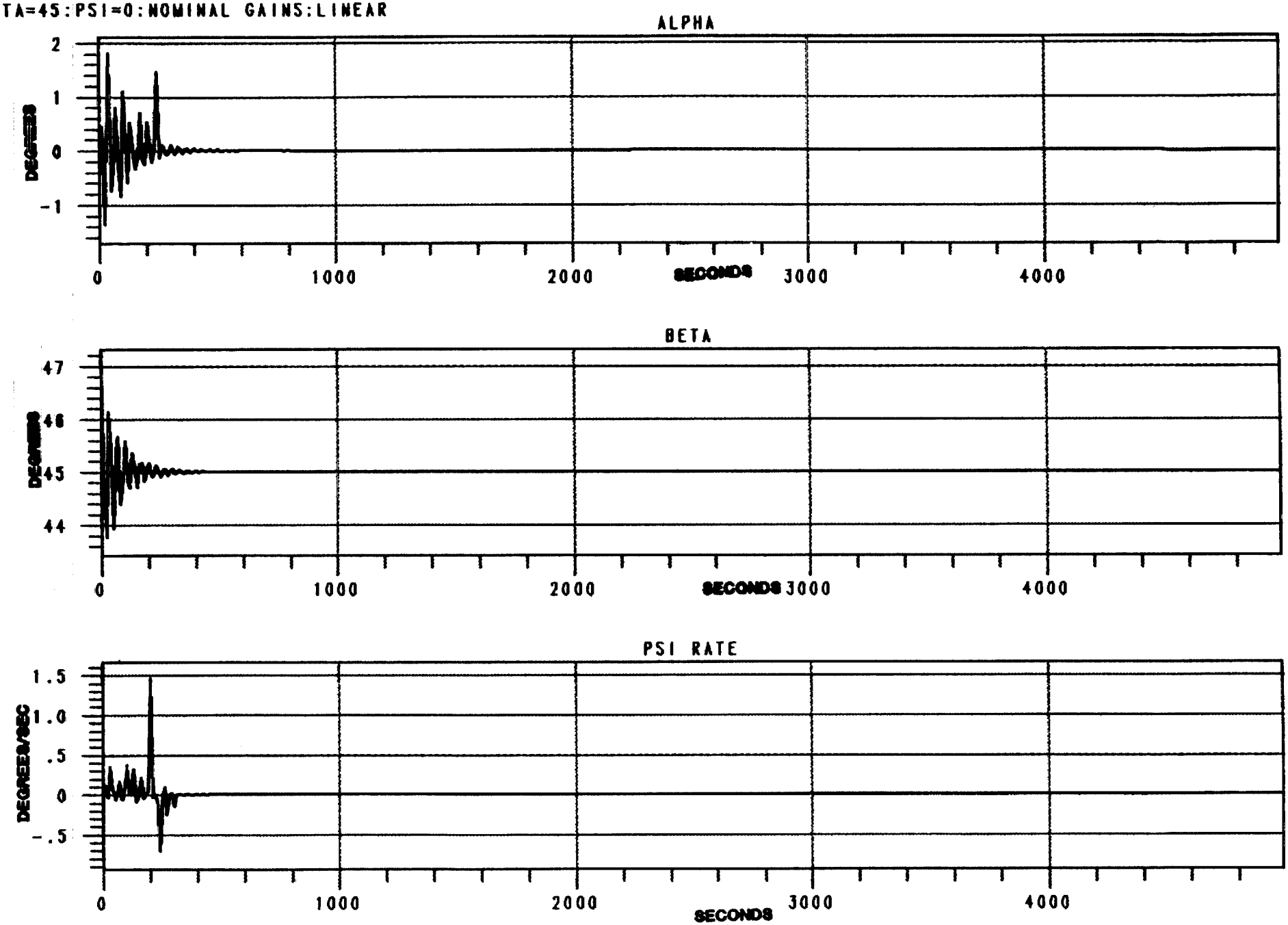

File: iUEBN.OUT

The time is 14:50:50.61 23-JUL-1989

BETA=91:PSI=0:NOMINAL GAINS:NON-LINEAR

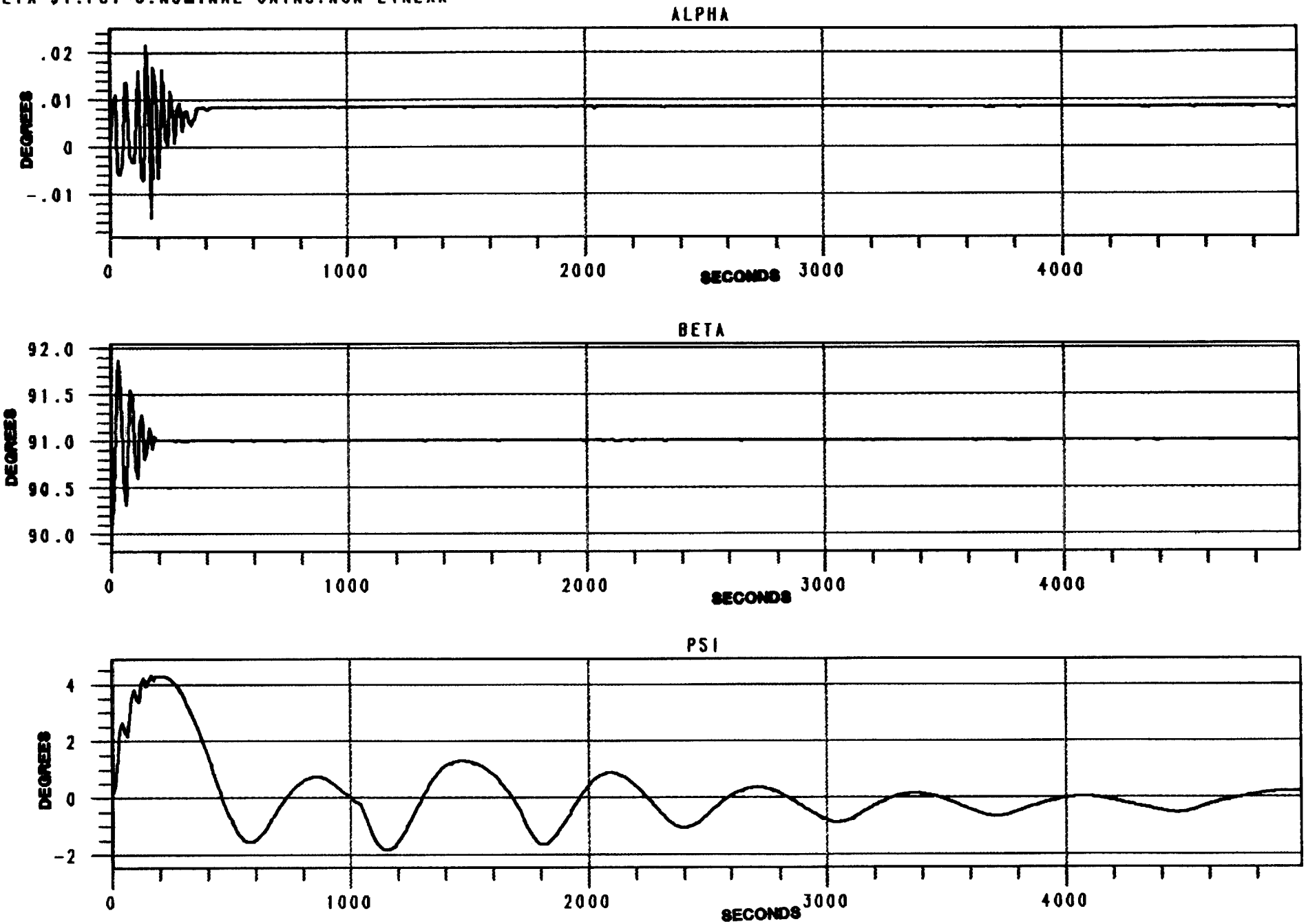

File: IUEBN.OUT

The time is 15:25:42.35 23-JUL-1988

BETA=45:PSI=0:NOMINAL GAINS:NON-LINEAR

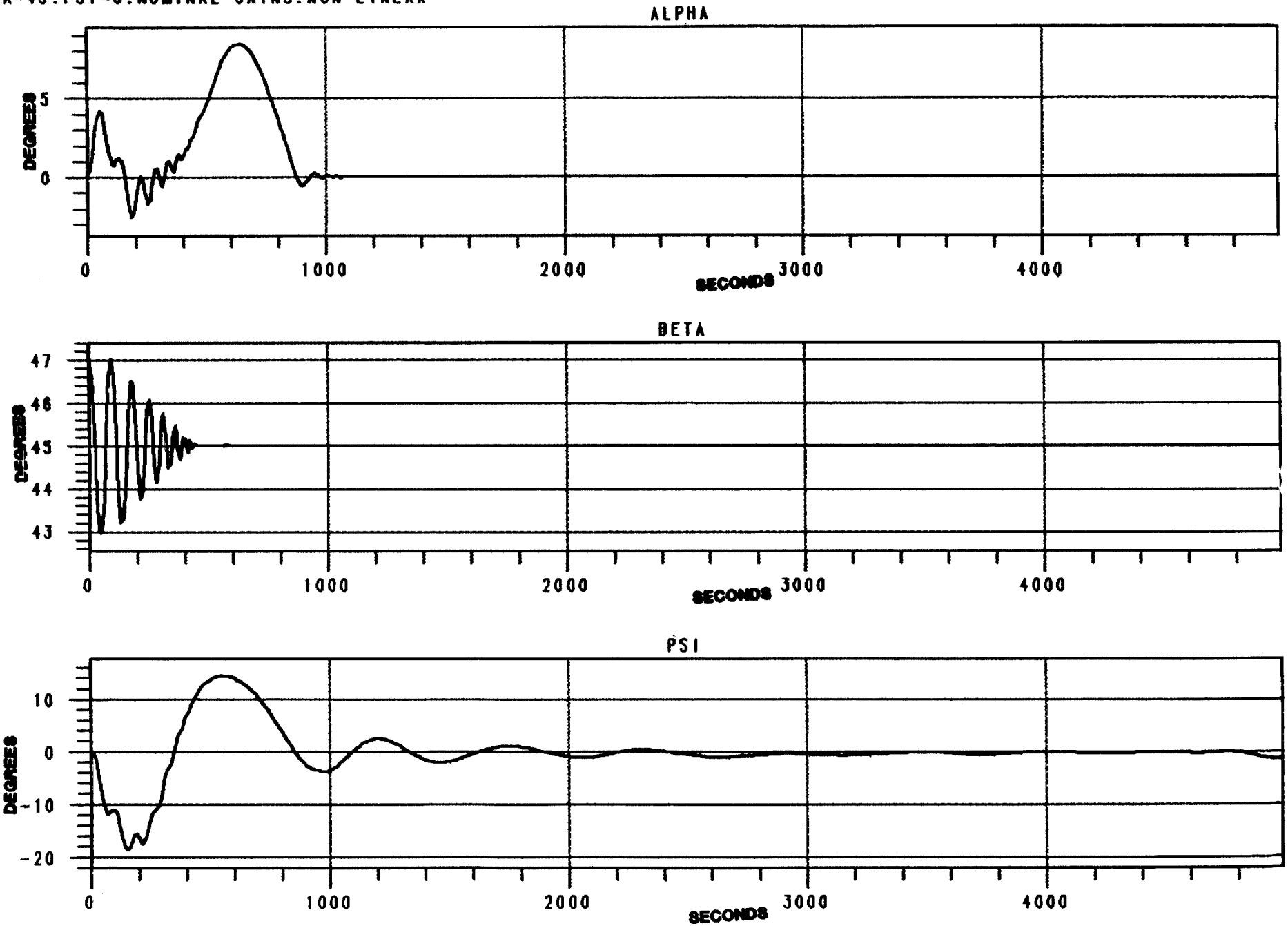

E10

File: IUEBN.OUT

The time is 13:58:54.27 24-JUL-1989

BETA=90:PSI=44:NOMINAL GAINS:NON-LINEAR CONTROLS

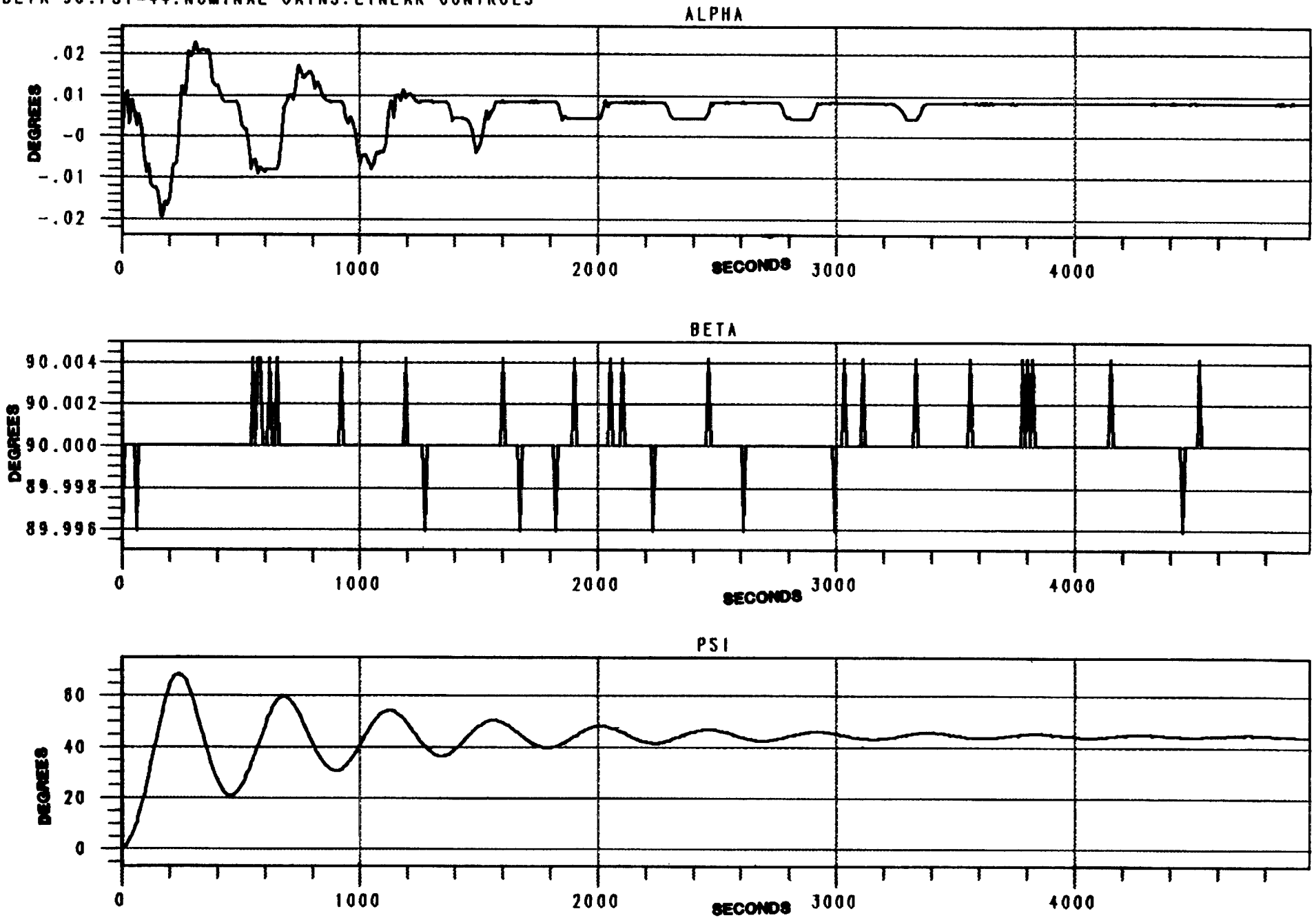

NASA
National Aeronautics and Space Administration

Report Documentation Page

1. Report No.	2. Government Accession No.	3. Recipient's Catalog No.
NASA TM-100748		

4. Title and Subtitle	5. Report Date
Analytical Derivation and Verification of Zero-Gyro Control for the IUE Satellite	November 1989
	6. Performing Organization Code: 712

7. Author(s)	8. Performing Organization Report No.
Tiffany Bowles and John Croft	89B00245
	10. Work Unit No.

9. Performing Organization Name and Address	11. Contract or Grant No.
Goddard Space Flight Center Greenbelt, Maryland 20771	
	13. Type of Report and Period Covered: Technical Memorandum
12. Sponsoring Agency Name and Address	14. Sponsoring Agency Code
National Aeronautics and Space Administration Washington, D.C. 20546-0001	

15. Supplementary Notes

16. Abstract The International Ultraviolet Explorer (IUE) satellite was launched January 26, 1978 into a geosynchronous orbit over South America. From its stationary position, the telescope maintains continuous communication with the control centers at NASA's Goddard Space Flight Center in Greenbelt, Maryland, and at the European Space Agency's (ESA's) Villafranca del Castillo Satellite Tracking Station in Spain. Since its launch in 1978, the satellite has gradually lost four of the original six gyroscopes in the Inertial Reference Assembly (IRA). In August 1985, the fourth of the original six gyros failed and a two-gyro system developed by NASA-GSFC was uplinked to the satellite and is currently in use. A one-gyro system also developed by NASA-GSFC is ready for use in case of another gyro failure. In the event that the sixth gyro should also fail, a zero-gyro system is being developed. The goal of this system is to provide inertial target pointing without the use of gyroscopes. The satellite has sun sensors to provide attitude information about two of the three axes. It relies upon the exchange of reaction wheel momenta to determine angular position and rate of the third axis.

17. Key Words (Suggested by Author(s))	18. Distribution Statement
International Ultraviolet Explorer, attitude gyros, satellite guidance, inertial reference systems	Unclassified - Unlimited Subject Category 18

19. Security Classif. (of this report)	20. Security Classif. (of this page)	21. No. of pages	22. Price
Unclassified	Unclassified	45	